- 1 3D Printing Assisted Surface Patterning Process on Acrylated Hydrogels for
- 2 Contact Guidance of Fibroblasts.
- 3 Amrita Natarajan<sup>#1</sup>, Suntae Kim<sup>#2,3</sup>, Gerardo Hernandez Moreno<sup>4</sup>, Jeroen Eyckmans<sup>2,3</sup>,
- 4 Christopher Chen<sup>2,3</sup>, Derrick Dean<sup>1</sup>, Vineeth M Vijayan<sup>1</sup>\*
- <sup>1</sup>Laboratory for Polymeric Biomaterials, Department of Biomedical Engineering, Alabama State
- 6 University, Montgomery, AL 36104, USA
- <sup>2</sup>Wyss Institute for Biologically Inspired Engineering, Harvard University, Boston, MA 02115,
- 8 USA
- 9 <sup>3</sup>Tissue Microfabrication Laboratory, Department of Biomedical Engineering, Boston University,
- 10 Boston, MA 02215, USA
- <sup>4</sup> Southern Research, Birmingham, AL 35294, USA.
- # These authors contributed equally,
- \*Corresponding Author Email: vviijayan@alasu.edu
- 14 Abstract: Generating stable and customizable topography on hydrogel surfaces with contact
- 15 guidance potential is critical as it can direct/influence cell growth. This necessitates the
- development of new techniques for surface patterning of the hydrogels. We report on the design
- of a square grid template for surface patterning hydrogels. The template was 3-D printed and has
- the diameter of a well in a 24-well plate. Hyaluronic acid methacrylate (HA) hydrogel precursor
- 19 solutions were cast on the 3D printed template's surface, which generated 3D square shape
- 20 topographies on the HA hydrogel surface upon demolding. The 3D Laser Microscopy has shown
- 21 the formation of a periodic array of 3D topographies on hydrogel surfaces. 3D Laser and Electron
- 22 Microscopy Imaging have revealed that this new method has increased the surface area and
- 23 exposed the underlying pore structure of the HA hydrogels. To demonstrate the method's
- versatility, we have successfully applied this technique to generate 3D topography on two more
- acrylate hydrogel formulations, gelatin Methacrylate and polyethylene glycol dimethacrylate.
- Human neonatal dermal fibroblast cells were used as a model cell line to evaluate the cell guidance

- 27 potential of patterned HA hydrogel. Confocal fluorescence microscopy imaging has revealed that
- the 3D surface topographies on HA hydrogels can guide and align the actin filaments of the
- 29 fibroblasts presumably due to the contact guidance mechanism. The newly developed
- 30 methodology of 3D topography generation in acrylate hydrogels may influence the cell responses
- on hydrogel surfaces which can impact biomedical applications such as tissue engineering, wound
- 32 healing, and disease modeling.
- 33 Total Word Count- 6363
- 34 Total Figures-8

37

38

39

40

41

42

43

44

45

46

47

48

49

50

51

52

35 Keywords: Hydrogels, Surface Patterning, Contact Guidance, Tissue Engineering

#### 1. Introduction

Hydrogels are three-dimensional crosslinked networks of polymers that can retain a large amount of water[1]. They are used for several biomedical applications such as drug delivery, tissue engineering, and wound healing[2]. Hydrogels formed from acrylate derivatives of polymers such as Hyaluronic acid Methacrylate[3], Gelatin Methacrylate[4], and Polyethylene Glycol Diacrylate[5] have received wide attention. This is mainly due to the acrylate bonds of natural and synthetic versions that can be crosslinked via photochemical or chemical strategies [5]. Acrylated hydrogels have wide utility for various biomedical applications such as bioink materials for 3D bioprinting, injectable scaffolds for tissue engineering, implantable drug delivery devices, and skin patches for wound healing[5, 6].

Hydrogel surface properties are critical for guiding cellular responses[7]. Most often, surface properties of the hydrogels such as surface roughness, surface area, and surface topography can impact/guide the cell responses[8]. Among the different surface cues, topography can play a major role in guiding cell responses[7]. This is mainly accomplished via contact guidance mechanisms. In the contact guidance process, cells receive active guidance signals from topographic cues such as grooves, ridges, or nano/micro patterns[9]. This impacts the different cell functions including proliferation, differentiation, and polarization[9].

Generating stable and customizable topography on hydrogel surfaces with contact guidance potential is very challenging and an area that needs active research[7]. Existing approaches for surface modification on hydrogels include but are not limited to photolithography[10], nanoimprint lithography[11], casting method[12], and 3D printing[13]. These methods have advantages and disadvantages. The lithographic technique, a common patterning method, requires a photomask that is not easily customizable and is not a cost-effective method[7]. Emerging methods like 3D printing show promise as they can print patterned hydrogels using computer-aided (CAD) software[13]. However, it is limited to only a few hydrogel formulations that meet the requirements of 3D printing. The casting method is one of the simplest and most effective methods to generate topographical patterns on hydrogel surfaces. Although a simple and effective method, this approach typically uses silicone molds which are not easily customizable. Also, there is a risk of the collapsing formed patterns due to excessive strains experienced by the mold material during the demolding process[7]. So a careful review of the literature shows that some of the existing challenges related to the generation of surface topography on hydrogel surfaces are (i) lack of customized templates/molds for generating the topographies, (ii) expensive nature associated with techniques such as photolithography, (iii) availability of very limited hydrogel formulations meeting the requirements of 3D printing, (iv) the stability issues of the patterns generated through simple techniques such as casting method and (v) finally the lack of scalability associated with these process. This very clearly suggests the importance of developing new surface topography generation processes on hydrogels that are simple, cost-effective, versatile, and scalable.

53

54

55

56

57

58

59

60

61

62

63

64

65

66

67

68

69

70

71

72

73

74

75

Inspired by these existing challenges associated with the generation of surface topographies on hydrogels, here we report a new method to generate 3D surface topography on hydrogels which

- is simple, cost-effective, and versatile. We have designed and 3D printed a 24-well plate-sized
- square-shaped Polylactic Acid (PLA) design. Up on casting with acrylated hydrogels such as HA,
- 78 GelMA and PEGDA has generated stable 3D surface topographies using this 3D printed PLA
- 79 template.

#### 2. Materials and Methods

- 81 Methacrylated hayluronic acid (HAMA), polyethylene glycol diacrylate (PEGDA), gelatin
- methacrylate (GELMA), 2-hydroxy methacrylate (HEMA), ammonium persulfate (APS) and
- ascorbic acid were purchased from Fischer Scientific. The polylactic acid (PLA) spool used for
- the 3D printing process was purchased from Flash Forge, United States.

## 2.1. Design of the 3D Printed PLA Template

- 86 Design requirements were formulated using an iterative approach with development being focused
- 87 on compatibility with a 24-well plate design using SolidWorks software. A Flash Forge Creator
- 88 Max Dual Extruder 3D Printer was used for all 3D printing processes. 3D printing was done using
- 89 1.75 mm Poly (lactic acid) filaments. The printing temperature was set to 200° C and the print bed
- 90 was set at 50° C. A travel speed of 60 mm/s along with a print speed of 30 mm/s was used.

# 91 <u>2.2. Preparation of Hydrogel Precursor Solutions</u>

- 92 Initially, 10 mg HAMA was dissolved in 10 ml of dPBS solution (concentration of 1mg/ml) to
- 93 prepare the HAMA precursor solution for the hydrogel preparation. The initiator for the hydrogel
- crosslinking Ammonium Persulfate (0.1M) was prepared by dissolving 114 mg of APS in 1 ml
- 95 dPBS solution (with a PH of 7.4). The catalyst for the crosslinking reaction Ascorbic Acid (0.1M)
- was prepared by dissolving 88 mg of Ascorbic acid in 1 ml dPBS solution.

# 2.3. Preparation of Non-Patterned Hyaluronic Acid (HA) Hydrogel

- The non-patterned HA hydrogels were prepared on a 24-well plate. Briefly, 400µl of hyaluronic acid methacrylate (HAMA) was added into a well followed by the addition of 200µl of 2-hydroxy ethyl methacrylate (HEMA) as the crosslinker. To initiate the free radical polymerization-induced crosslinking, 100µl of APS and Ascorbic acid were added quickly.
- 2.4. Preparation of Surface Patterned Hyaluronic Acid (HA) Hydrogel
- To prepare the Surface patterned HA gel, we have placed the 3D-printed PLA mold inside the well of a 24-well plate. 400µl of Hyaluronic acid methacrylate (HAMA) was added on the top of the template followed by the addition of 200µl of 2-hydroxy ethyl methacrylate (HEMA). To initiate the free radical polymerization-induced crosslinking, 100µl of APS and Ascorbic acid were added quickly.
- 2.5. Preparation of Non-Patterned and Surface Patterned Gelatin Methacrylate (GelMA) and
- 109 Polyethylene Glycol Diacrylate (PEGDA) Hydrogels
- 110 The non-patterned HA hydrogels were also prepared on a 24-well cell culture plate. Briefly, 400μl of GelMA (1mg/ml stock solution) and PEGDA (3 mg/ml stock solution) were added into separate wells followed by the addition of 200μl of 2-hydroxy ethyl methacrylate (HEMA) as the crosslinker. To initiate the free radical polymerization-induced crosslinking, 100μl of APS and
- 114 Ascorbic acid were added quickly.
- 115 The surface patterned GelMA and PEGDA hydrogels were formed using the same procedure with
- the difference of casting the solutions over the 3D printed PLA template to generate surface
- topography.

97

98

99

100

101

# 118 2.6. Characterization of the Hydrogels 119 The viscoelastic behavior of the hydrogels was measured using a TA Instruments Discovery HR-120 2 Rheometer. The surface features of surface patterned& non-patterned HA gels were studied using 121 3D Laser Scanning Confocal Microscope VK-X1000. The surface areas of the surface patterned, and non-patterned hydrogels were measured using VK-X3000 3D Surface Profiler feature of the 122 123 Keyence Microscope. The surface topography of the hydrogels were performed using a Phenom XL Benchtop Scanning Electron Microscope. 124 2.7. Plasma Surface Modification of the Hydrogels 125 126 The surface-patterned and non-patterned hydrogels were surface-modified using a Harrick Plasma 127 chamber. More specifically, hydrogels were placed inside the chamber with an airflow rate of 20 128 sccm and subsequently, plasma was ignited after applying a radiofrequency of 13.56 MHz and 45 W for 5 minutes. 129 130 2.8. Cell culture Human neonatal dermal fibroblast was purchased from Lonza(CC-2509). The fibroblast grew in 131 132 FGM<sup>TM</sup>-2 Fibroblast Growth Medium-2 BulletKit<sup>TM</sup>(Lonza, CC-3132) under 37°C, 95% humidity, and 5% CO2 conditions. All the cells were used in passages 3-5 and the media was 133 replaced every other day. 134 2.8.1. Cell adhesion experiment on HA gels 135 136 Physical collagen coating on the hydrogels was conducted before seeding the fibroblasts. Fully swollen HA gels were sterilized by emitting UV light for 15 minutes each on both sides. The sterile 137

hydrogels were placed into 24 well plates and soaked overnight at 4° C in 200 μg/ml collagen type

I solution (Corning, 356236) diluted with DI water. The hydrogels were washed with PBS 3 times right before seeding the fibroblasts. When the fibroblasts reached around 80% confluency, the cells were washed with PBS and enzymatically detached (0.05% trypsin/EDTA). 2x 10⁴ cells for low density and 1 × 10⁵ cells for high density were seeded in each well plate with 1ml of media. For actin staining and imaging, the hydrogels were fixed with 4% paraformaldehyde (Electron Microscopy Sciences, 15710) for 30 min at specific time points after seeding(3,6,24,48h). After blocking with 2% BSA in PBS for 1h at room temperature, Alexa Fluor™ Plus 555 Phalloidin(Thermofisher Scientific, A30106, 1:1000), and DAPI (Sigma, D9542, 1:1000) were incubated for 2h at room temperature. The samples were washed with PBS between each step. Confocal and 3D images were acquired with a Leica HC FLUOTAR L 10x and 40x water-immersion objective on an upright TCS SP8 multiphoton microscope (Leica)

# 2.8.2. Quantification of actin images by ImageJ

We quantified cell area, orientation coherency, and orientation distribution by using the "measure", "directionality" and "OrientationJ" plug-in in ImageJ as described previously[14]. Mean intensity and cell area were simply measured by the "measure" function after setting the scale for 40x image (n=20). For coherency and distribution analysis, all the actin images were rotated to match the most aligned actin filament to 0 degrees using the horizontal alignment function in Orientation J. Then, the "dominant direction" function in Orientation J was utilized to calculate orientation coherency from 0 (no alignment) to 1 (perfect alignment) (n=6). The orientation distribution data of actin can be obtained by the "directional" function with the Fourier component method.

## 2.9. Statistical Analysis

One-way ANOVA was conducted to analyze the differences between patterned and no pattern groups. For the group analysis over time, two-way ANOVA was employed to compare the mean values. From \*P < 0.05, it is considered to have statistical significance. (n.s., not significant, \*P < 0.05, \*\*P < 0.01, \*\*\*P <0.001, \*\*\*\*P<0.0001.) Statistical analyses were performed using GraphPad prism. All data points on the graphs represent average values, and error bars depict the SEM.

### 3. Results and Discussion

160

161

162

163

164

165

166

167

168

169

170

171

172

173

174

175

176

177

178

179

180

181

182

The major interest of this work was to develop a simple, cost-effective, and versatile method to generate 3D surface patterning method on hydrogel surfaces. 3D printing thermoplastic polymers like Polylactic Acid is one of the most cost-effective methods in additive manufacturing. Inspired by this, we decided to use a 3D-printed PLA template design to guide the generation of topographies on hydrogel surfaces. We hypothesized that the usage of a custom 3D printed mold for casting the hydrogel solutions would generate negative impressions of the positive mold material. To test this hypothesis, we have manufactured a 3D-printed square grid using a fused deposition modeling technique using PLA. The dimensions of the 3D design iterations were based on 24-well polystyrene plates used for cell culture. We first measured the dimensions of a 24-well plate and used that as a baseline to design the PLA template. The printed PLA construct has a diameter of 15 mm with each square in the grid pattern measuring 1mm fitting well within a 24well plate (Figure 1a). The rationale behind printing a 24-well plate size design was to generate surface-patterned hydrogels which can easily facilitate in vitro cell studies. Usually, to perform in vitro testing using biomaterials, researchers often need to cut or manipulate their material constructs to be used for cell culture well plates to allow for the proximity of the material to the cell monolayer[15]. Other groups grow their cell model on their respective materials and then are

required to detach the cells for analysis in separate dishes[16] or well plates[16, 17]. This is inconvenient and can be an issue related to time and material waste concerning critical cell-based assays for analysis of biocompatibility. Hence, designing surface patterned hydrogel that exactly fits the size of a cell culture well plates will be an efficient method to generate more reliable and consistent results with cell studies.

The confocal laser surface scanning microscopy showed a clear transfer of the mold pattern from the design to the printed structure (Figure 1b). The square grid-type pattern was observed from the images with closed cavities which can hold hydrogel solutions while casting (Figure 1c,d). Subsequently, we have used Methacrylated Hyaluronic Acid (HA) as the precursor for HA hydrogel formation. The experimental plan for generating the surface-patterned HA hydrogel using the casting method on the template/mold was shown schematically (Figure 1e). More specifically, hydrogel solution along with crosslinkers and initiator will be cast on the PLA template which forms a hydrogel and upon demolding would generate negative impressions of the positive mold material.

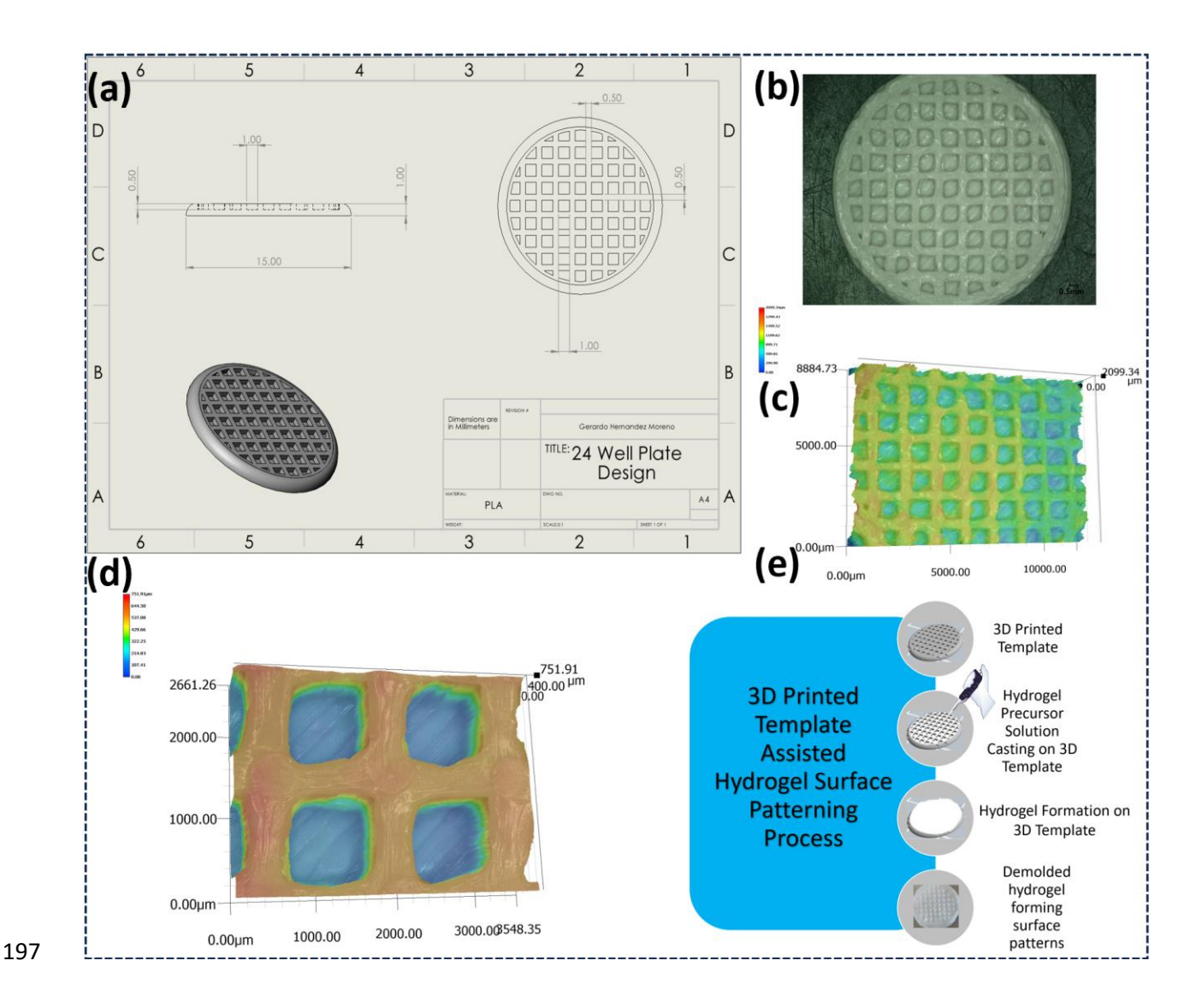


Figure 1: Design Iteration of the 24 well plate sized PLA template from SolidWorks Software (a), Laser Surface Scanning Microscopy Images of the 3D printed PLA template (b-d), 3D Laser Scanning Microscopy Images of the 3D, the schematics of the 3D printed template assisted process (e).

The hydrogel-forming solutions were poured on the mold and placed inside a 24-well plate. We have observed that with time there was a development of turbidity inside the wells which is an indication of the crosslinking process (Figure 2a). The mechanism of hydrogel formation was based on a free radical-initiated chemical crosslinking process. (Figure 2b). Specifically, the unsaturated double bonds of the methacrylated hyaluronic acid were crosslinked using another unsaturated vinyl monomer 2-Hydroxy ethyl methacrylate (HEMA) using a radical initiator

Ammonium Persulfate. The rationale behind using the free radical-initiated chemical crosslinking process was to generate hydrogels with strong mechanical properties. Conventionally in the surface patterning process, researchers use photo crosslinking of methacrylated polymers such as HA, GelMA, and PEGDA which is found to provide weaker mechanical properties to the resultant hydrogels[18]. So, we anticipated that the strong chemical crosslinking process will provide the necessary strength to our hydrogels which can withstand the stress associated with the demolding process without collapsing the patterns.

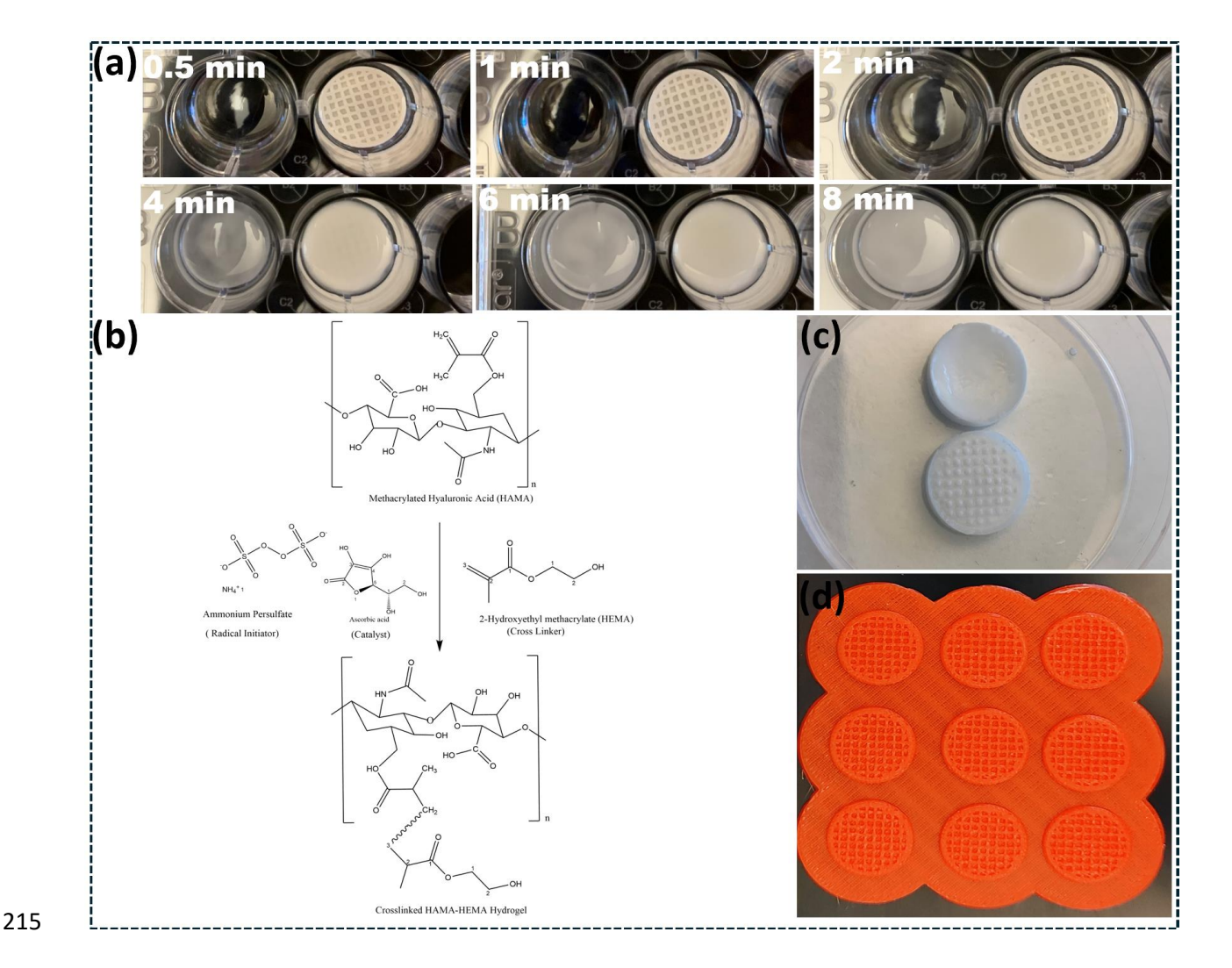


Figure 2: The images showing the comparison of the hydrogel formation on the plain 24-well plate and the top of the 3D template at different time points (a), the chemical crosslinking process of the Hyaluronic Methacrylate and 2-Hydroxy Ethyl Methacrylate forming the HA hydrogel (b), the

photographs of the non-patterned and patterned hydrogels after the crosslinking process (c), image of the nine 3D printed PLA template structures (d).

219220

221

222

223

224

225

226

227

228

229

230

231

232

233

234

235

236

237

238

239

240

241

242

After the crosslinking process, we carefully demolded/removed the hydrogel from the PLA mold resulting in the production of HA hydrogels with stable surface patterns which are the negative impressions from the positive mold material (Figure 2c). The scalability of the 3D printing was demonstrated by printing 9 designs together with consistency (Figure 2d). This is another advantage of this process compared to PDMS-based molds in photolithography which are not easily customizable and scalable for surface patterning[19].

The FTIR spectra comparison has shown a decrease in the C=C stretching peak (1645 cm<sup>-1</sup> 1) intensity for the final crosslinked hydrogel in comparison with the HA and HEMA, this suggested the chemical crosslinking process of double bonds during hydrogel formation (Figure S1). Next, we have performed rheology measurements to identify important parameters such as the stiffness and the gelation time of the hydrogels. Time sweep experiments have shown that at 375 seconds the gelation process starts occurring which was evident by the increase in complex viscosity and cross-over between the storage and loss modulus of the hydrogels (Figure 3a). The frequency sweep experiments of the HA hydrogels were conducted to measure the storage modulus of the hydrogels. The results of the frequency seep experiment have demonstrated a higher storage modulus value of 1000 kPa for the HA hydrogel (Figure 3b). Generally, the Hyaluronic Acid Methacrylate is photo-crosslinked using initiators like Irgacure to produce HA hydrogels. However, the storage modulus of these photo-crosslinked HA hydrogels is relatively weak in the range of 10-100 Pa [20]. However, our present chemically crosslinked HA hydrogel displayed a very high storage modulus value which was several folds higher than the conventional photocrosslinked HA hydrogel formulations. This observed significant increase in the strength of the prepared HA hydrogel can be attributed to the strong chemical crosslinking process. This high stiffness of the HA hydrogels supports the generated topographies and provides stability to the formed patterns without collapsing after the demolding process from the PLA template.

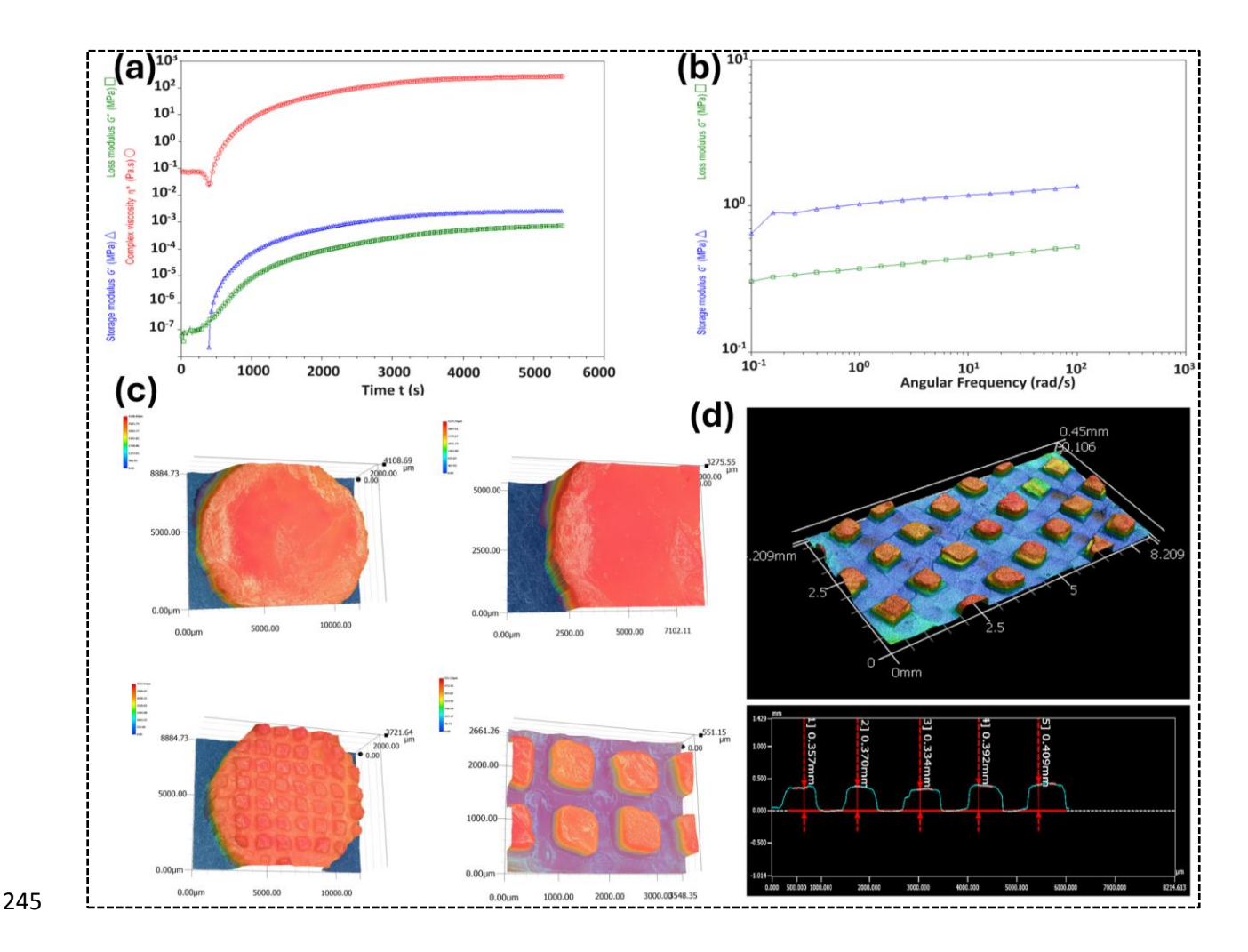


Figure 3: Rheological Measurements of HA hydrogels, time sweep experiments(a), frequency sweep experiments (b). 3D Laser Scanning Microscopy Images of the patterned and non-patterned hydrogels (to increase the contrast of the image food color dye was added on the hydrogel before taking the images) (c), Images showing the quantification of the width and height/depth of the square patterns formed on the surface of the HA hydrogels using the surface profiling measurements (d).

Images from the 3D laser confocal microscopy showed the periodic 3D array of square-shaped topographical patterns formed on the hydrogel surface (Figure 3c). More specifically, the surface of the hydrogel was composed of square-shaped pillars with periodic interspacing between the pillars throughout the entire surface of the HA hydrogel. The average surface area of the HA

hydrogel was measured using the surface profiling feature of the 3D laser confocal scanning microscopy by selecting 17 different spots on the patterned hydrogel (Figure S2). The average surface area of the patterned hydrogel was found to be 0.760 mm<sup>2</sup>. In the case of un-patterned hydrogel surface, a completely flat surface topography was observed with an average surface area of 0.007 mm<sup>2</sup>. Thus, it was clear that the 3D printed patterned molds introduced surface patterning and increased the overall surface area of the HA hydrogel. The 3D surface profiling of the hydrogels showed the average height and width of the square pillars to be 311 and 870µm (Figure 3d). The actual 24-well plate PLA template/mold has a depth of 500 µm and a pore width of 1000 um. Hence, the expected height and width of the square patterns formed on the hydrogel surface should be around 500 and 1000 µm. However, the observed height and width of the square patterns (311 and 870µm) were lower than these values. This difference may be attributed to the printing resolution issues with the 3D printer. Improving the printing resolution may create a closer alignment in the height and width of the square patterns in the design and hydrogel constructs. The reported observations corroborated our initial hypothesis by printing 2 more additional PLA templates with pore widths of 2000 and 3000 µm. Casted HA hydrogels were poured on its surface and subsequently demolded. As the pore width of the template increased the uniformity of the square shape generated on the hydrogel surface significantly improved (Figure S4). This observation suggested that printing low pore width templates is challenging and needs more systematic optimization of printing parameters such as print speed, nozzle diameter and nozzle temperature. As low size and higher number of surface patterns are critical for governing the cell response such as those that arise from increased surface area, we have chosen the 1000 µm template mold patterned hydrogels for further studies.

256

257

258

259

260

261

262

263

264

265

266

267

268

269

270

271

272

273

274

275

276

Subsequently, we have taken the Scanning Electron Microscopy images of the patterned vs non-patterned HA hydrogels. Interestingly, it was seen that the hydrogels with the 3D surface topography exposed the underlying porosity than the non-patterned ones (Figure 4). This difference in the pore structure could be attributed to the square cavity structures of the PLA mold. More specifically, on the flat 24-well plate surface, the hydrogel precursor solutions (the polymer, crosslinker, initiator, and catalyst solutions) form a continuous film whereas inside the mold there is a non-continuous and confined distribution of hydrogel precursors are present which can impact the formation of hydrogels on the template.

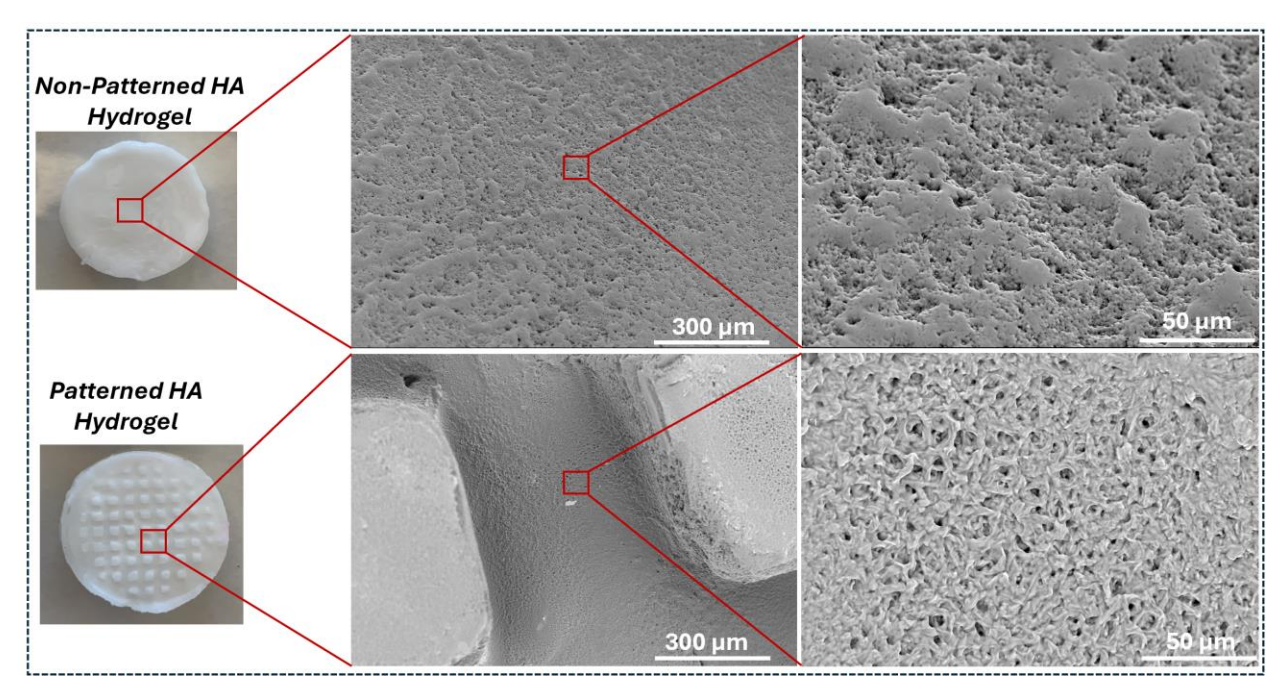


Figure 4: The Scanning Electron Microscopy Images showing the topography and pore structure of Hyaluronic Acid Methacrylate Hydrogels formed on the flat 24 well plate versus 3D printed PLA template surface

We speculate that the formation of hydrogel on the template will be impacted by the hydrostatic pressure caused by the square-shaped cavities of the mold. This is because each square cavity of the PLA mold has an average depth of 650µm (Figure S3). This may contribute towards the generation of hydrostatic pressure on the hydrogel precursor solutions proportional to the

depth. Non-patterned hydrogels are formed by casting the hydrogel solution on a plain surface of the 24-well. More in-depth quantitative experiments are needed to validate this speculation and our future studies will attempt to address it. Hence, we believe that these factors of confined non-continuous distribution of the hydrogel-forming solutions and the possibility of experiencing hydrostatic pressure on the templates could have impacted the pore structure of the hydrogels in comparison with hydrogels formed on the flat 24-well plate surface. This shows the positive impact of the template material on exposing the pore structure of the hydrogel.

Method versatility was shown by applying the same 3D printed mold to other methacrylate hydrogel-forming materials Gelatin Methacrylate (GelMA) and Polyethylene Glycol Diacrylate (Figure S5). The SEM images of the patterned hydrogels of both GelMA and PEGDA showed the clear formation of a square pattern with more exposed pores compared to non-patterned ones. This observation supports the role of hydrostatic pressure on the pore structure of the hydrogel regardless of its composition. To assess the capability of the 3D topographies generated on the hydrogel surfaces, we have conducted cell attachment studies on HA hydrogels.

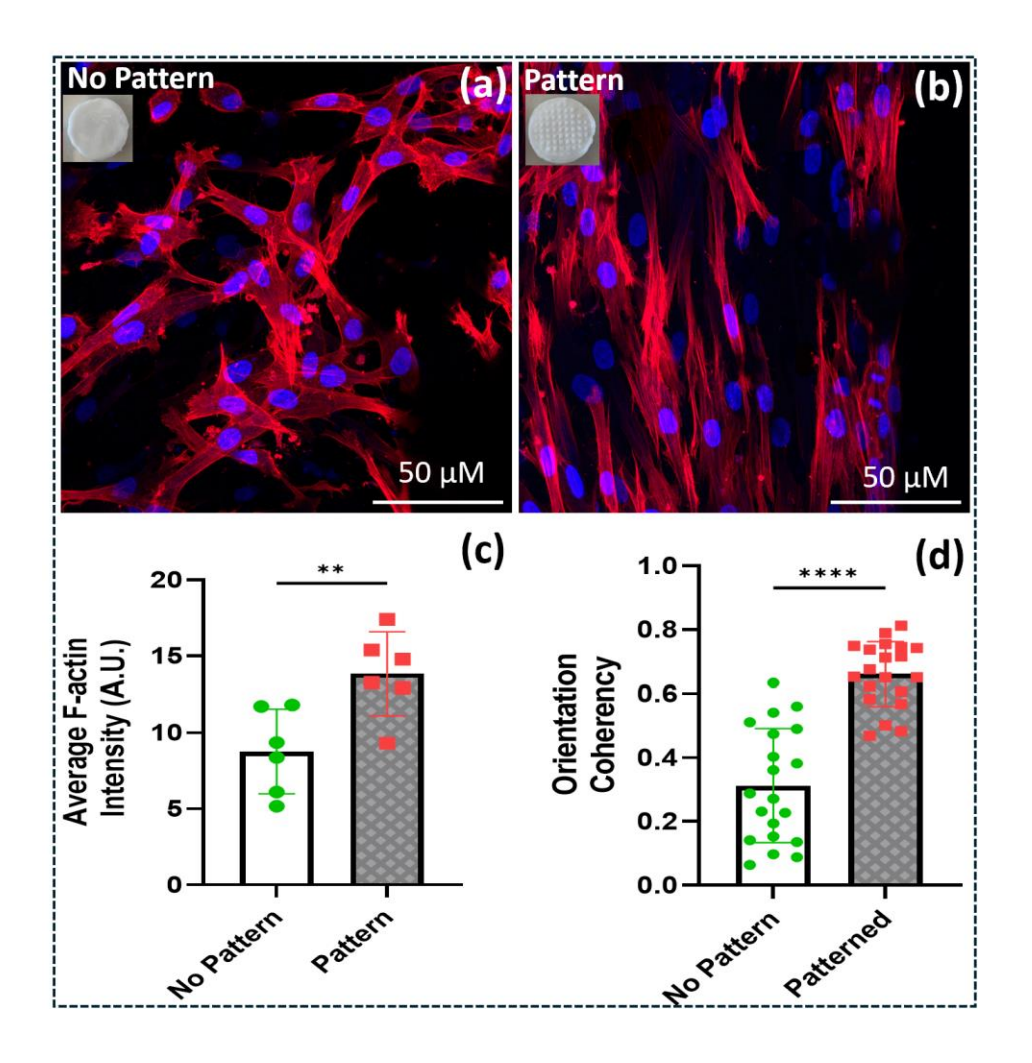


Figure 5. Fluorescent visualization of fibroblast of low density on collagen-coated HA gel without and with a surface pattern (a, b). Fluorescence images of F-actin (red) and nuclei (blue) stained human dermal fibroblast at 2 hours. (scale bars represent 50  $\mu$ m for 40x). Analysis of F-actin intensity and orientation coherency of single cells measured with ImageJ. (c, d) 0 means no alignment and 1 is perfectly aligned Measurement and comparison of the change in cell (\*P < 0.05, \*\*P < 0.01, \*\*\*P < 0.001, \*\*\*\*P < 0.0001)

For the cell studies, HA hydrogels were fabricated using the square grid pattern and demolded to get the surface-patterned hydrogels. The PLA template used to generate the patterns was discarded immediately after the generation of the surface patterns and only surface-patterned HA hydrogel samples were used to conduct cell attachment studies. Prior to the cell attachment studies, hydrogels were subjected to plasma treatment[21] and collagen coating[22]. This was to provide sterilization and facilitate better fibroblast attachment. Initially, we used a low fibroblast

seeding density to study the effect of topography on cell attachment. Fluorescence microscopy images of fibroblasts on surface-patterned hydrogels at the 2-hour time point showed increased Factin intensity and alignment compared to control non-patterned hydrogels (Figure 5 a&b). To get more quantitative insight into the alignment process, we have measured the fluorescence intensity and orientation coherency of the F-Actin filaments at a single-cell level on patterned and nonpatterned hydrogels (Figure 5c&d). We have observed a higher orientation coherency at the initial time point for patterned hydrogels which was indicative of the alignment of F-Actin filaments on patterned hydrogel surface. It was seen that the F-Actin filaments and the nuclei of the cells were aligned in a vertical/horizontal direction. It is important to note that the hydrogels are patterned using a template having a grid pattern that has each individual square arranged identically in both vertical and horizontal directions with similar dimensions and spacing (Figure 1a&b). The SEM image of the patterned hydrogel shows the 2 adjacent square topographies formed in the horizontal direction showing the position and spacing of the topographies consistent with the grid template (figure 4). The low cell seeding density fluorescent images of the patterned surfaces showed an orientation of the F-Actin and nuclei of cells in a vertical/horizontal direction consistent with the directionality of the grid patterns of the template. As the squares are identical in both vertical and horizontal directions in the template, we believe that there will be an equal probability for orientation in vertical/horizontal directions.

321

322

323

324

325

326

327

328

329

330

331

332

333

334

335

336

337

338

339

340

341

342

343

The surface-patterned hydrogel has a significantly higher surface area (0.760 mm²) compared to the control non-patterned hydrogel (0.007 mm²) in 3D topography imaging (Fig S2), this result suggested hydrogel with a large surface area facilitates initial cell attachment. This effect is likely due to the larger surface area providing a higher density of functional groups that cells can recognize and bind to and facilitating mechanical interlocking between cells and substrate[23].

This enhances physical anchoring and stability, thereby improving cell-topography interactions through contact guidance.

344

345

346

347

348

349

350

351

352

353

354

355

356

357

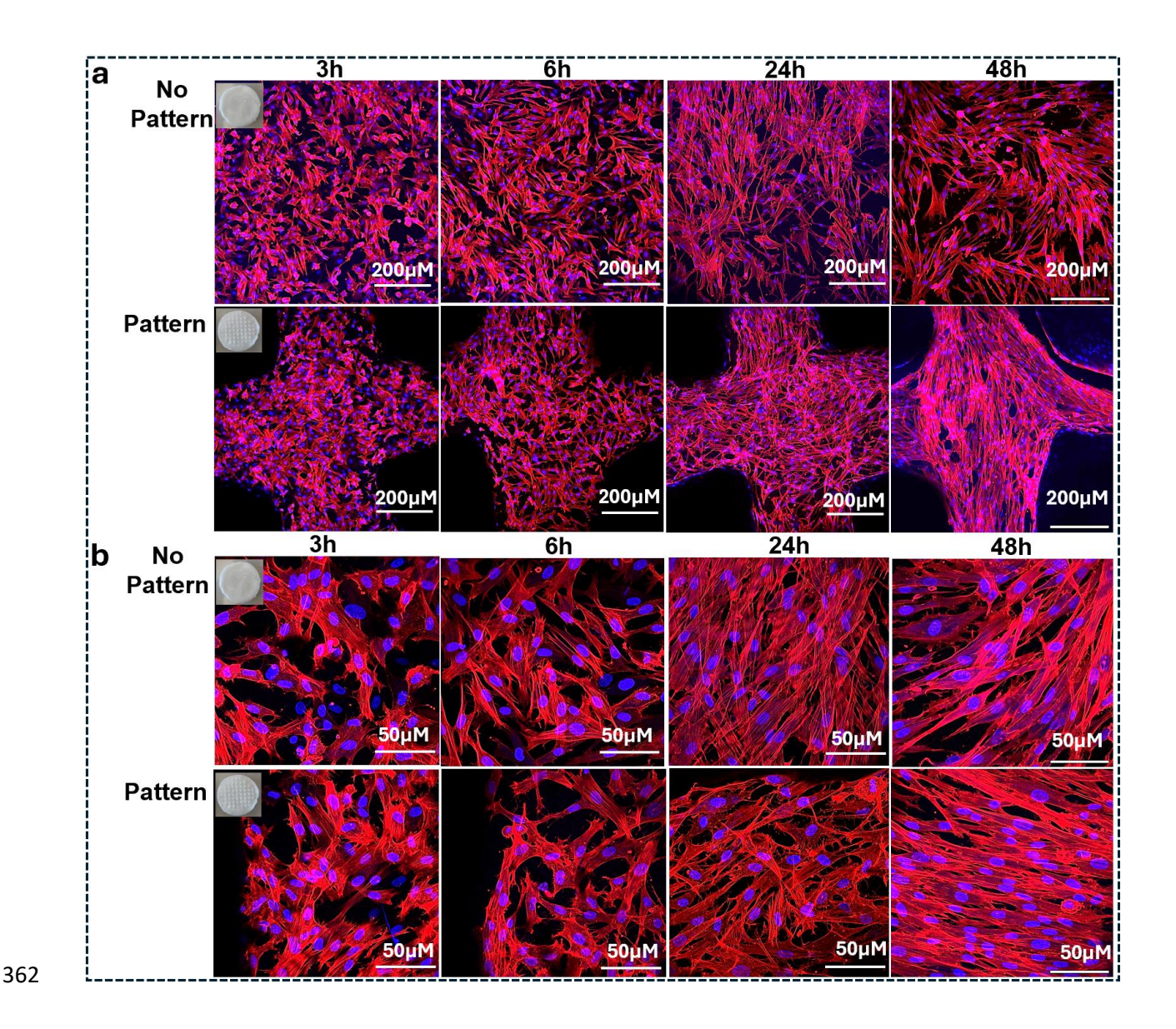
358

359

360

361

Subsequently, we have also analyzed cellular growth at different time intervals such as 3, 6, 24, and 48h with high cell density (Figures 6a&b). Previously, we observed differences in initial cell attachment based on surface patterns. Further, this study was conducted to evaluate the longterm impact of cellular growth on the tissue-level orientation capabilities of the patterned hydrogels. The multiphoton confocal fluorescence images of the cytoskeleton and nuclei arrangement of the dermal fibroblasts (F-actin in red and cell nuclei in blue) cultured in the patterned and non-patterned hydrogels were qualitatively and quantitatively analyzed after 3h, 6h, 24h, and 48h. The patterned HA hydrogel surface consists of repeating square pillars with periodic interspacing. Notably, fibroblasts were confined to the flat grooves between the pillars. Confocal fluorescence imaging at 10x magnification showed fibroblasts forming a cross-like pattern within these grooves (Figure 6a). In contrast, fibroblast attachment on the control un-patterned hydrogel was random without any confinement. Hence, it was clear that the topography formed on the hydrogels provided a confined/closed growth pattern to hydrogels. This showed the impact of the topographies on fibroblast response. It was already reported that small-scale microtopography and patterning could impact the growth pattern of the cells [23, 24]. However, these low-magnification images do not show any orientation/alignment of the cells in the patterned hydrogels at 3 and 6h.



and without a surface pattern: Fluorescence images of F-actin (red) and nuclei (blue) stained human dermal fibroblast over time (1,2,3,6,24,48h) at 10 and 40X magnifications with and without a pattern (a, b).

The higher magnification confocal fluorescence microscopy images (40X) were taken and compared for both patterned and non-patterned hydrogels to examine the F-Actin orientation of fibroblasts grown on patterned and non-patterned hydrogels (Figure 6b). The quantitative orientation coherency calculation shows that the orientation of cells was not significant for both types of patterned and non-patterned hydrogels at early time points 3,6 and 24h (Figure 6a&b).

Figure 6: Fluorescent visualization of fibroblast of high density on collagen-coated HA gel with

However, after 48h, there were significant disparities in the shape, morphology, and orientation of cultured cells within the patterned hydrogel was observed (Figure 6a&b).

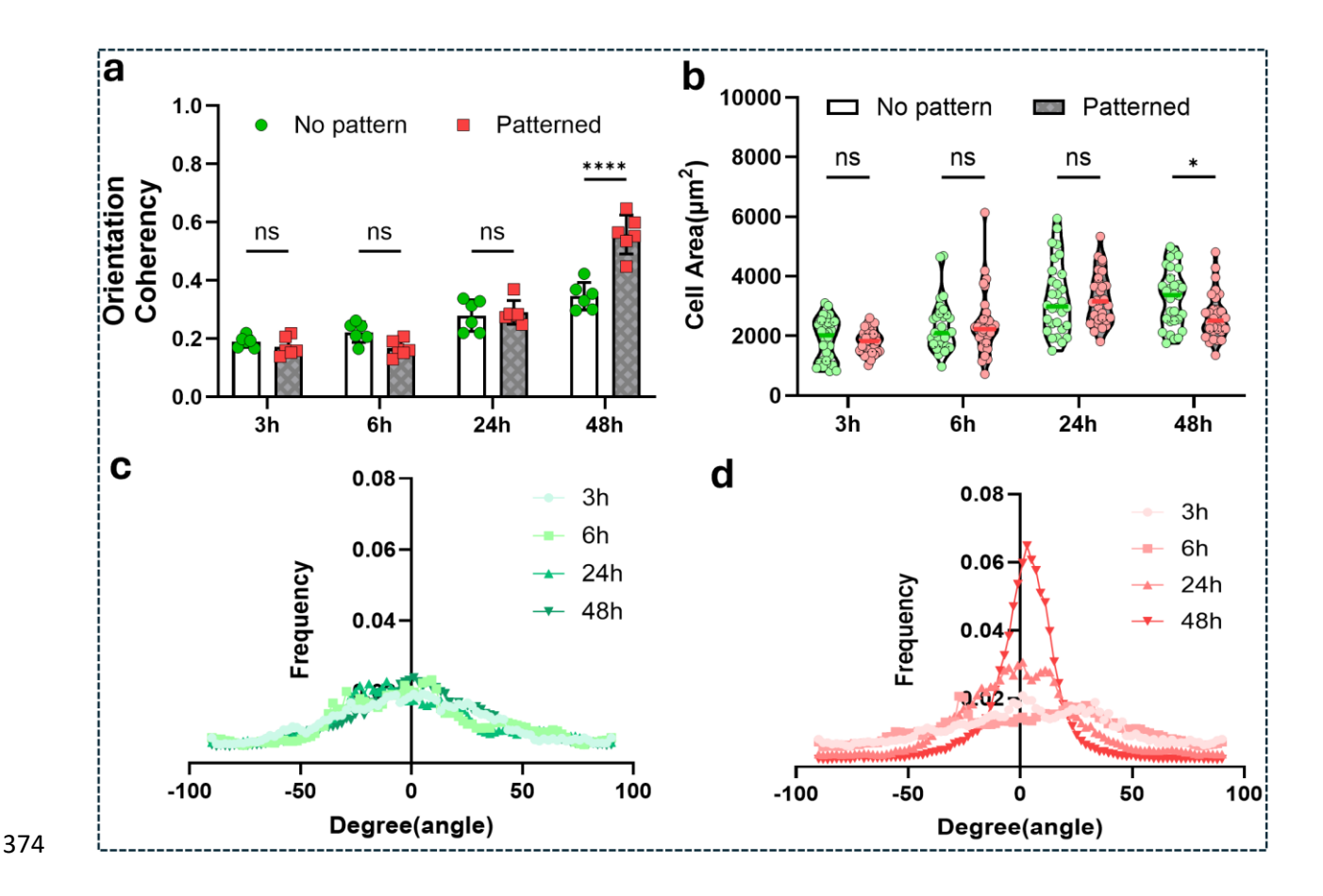


Figure 7: Analysis of orientation coherency calculated by directionality plug-in in ImageJ. 0 means no alignment and 1 is perfectly aligned (a), Measurement and comparison of the change in cell area over time for no pattern and patterned HA gel (b), Orientation distribution of stained F-actin on (c) no pattern and (d) pattered gels over time (n.s., not significant, \*P < 0.05, \*\*P < 0.01, \*\*\*P < 0.001, \*\*\*P < 0.0001).

More specifically, over time progression, there was an augmentation in the cell area up to 24h, attributed to cellular spreading and stable adhesion to the substrate. The cytoskeletal organization of cells on patterned hydrogel exhibited pronounced orientation coherency, particularly evident at the 48-hour time point in contrast to the non-patterned counterpart (Figure 7a). However, a reduction in cell area was observed specifically in the patterned hydrogel at 48h which cell alignment was actively observed (Figure 7b). Additionally, the frequency distribution graph

illustrated a distinct alignment pattern of actin filaments exclusively on the patterned hydrogel at 48h (Figure 7c, d).

The observed alignment of the fibroblasts on the patterned hydrogel at a longer time of 48h could be attributed to the increased cell-topography interaction and cell-cell interactions. More specifically, the observed confined growth of the cells through the grooves of the square patterns is expected to increase with time which can result in a more confined/narrow arrangement of cells. This was evident by the low magnification fluorescence image comparison of patterned and nonpatterned hydrogels at 3,6,24 and 48h (figure 6a). It was seen that the confined/narrow cell arrangement progressively increased with time and reached the maximum at 48h as evidenced by the most confined F-Actin and nuclei arrangement. Based on this observation, we believe that there is an increased topography-cell interaction at 48h. Also, it is very important to account for the high cell-cell interactions that may be present at a longer time point of 48h which can also contribute to the observed alignment process. Hence, we believe that there is a combinatory effect of topography-guided confined growth and increased cell-cell interactions which results in the observed alignment of the cells at 48h. More detailed investigations should be conducted to fully explore the exact mechanism behind this phenomenon and our future studies will aim to explore this.

Z stack confocal imaging was used to examine the three-dimensional distribution of cells on patterned hydrogels. At 48 hours, It was seen that cells displayed oriented intracellular actin filaments and aligned along the grooves of the patterned hydrogel-forming a cross-like pattern whereas for the non-patterned hydrogel, there was no observation of confined growth or alignment.

(Figure 8).

386

387

388

389

390

391

392

393

394

395

396

397

398

399

400

401

402

403

404

405

406

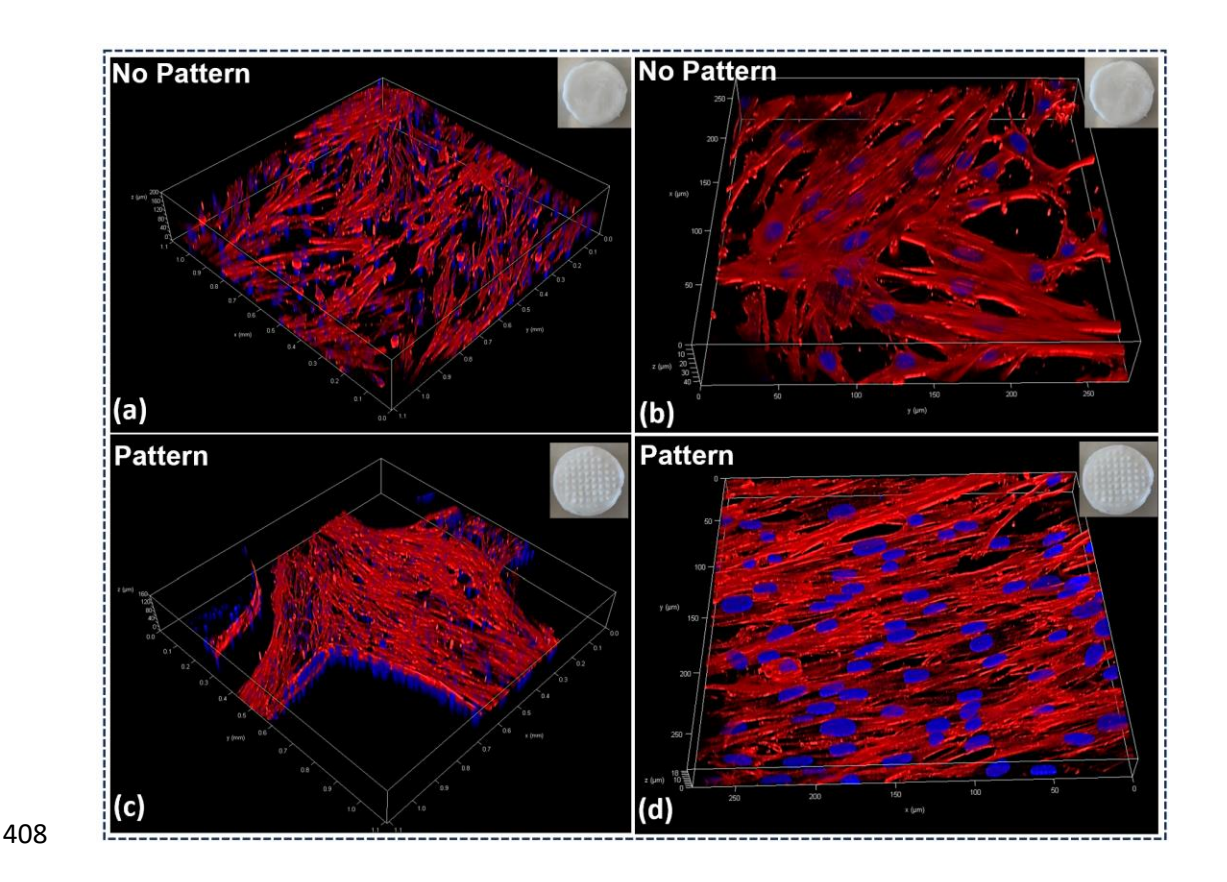


Figure 8: Z stack 3D Confocal Fluorescent images of the collagen-coated HA gel with and without a surface pattern. The images show F-actin (red) and nuclei (blue) stained human dermal fibroblast at 48h time points taken at different magnifications, 10X(a,c) and 40X (b,d).

These results indicate that a higher fibroblast density on patterned hydrogels facilitates a more rapid orientation of F-Actin filaments at the tissue level. Cellular alignment at the tissue level was not observed during the initial stages, likely due to the combined effects of intercellular and cell-substrate interactions under high-density conditions. However, as fibroblasts enter the proliferation stage over time, cellular alignment at the tissue level becomes clearly observable at 48 hours. It was previously reported that cells on substrates with porous and larger surface areas demonstrated increased migration velocity[25], and are more conducive to cell proliferation compared to flattened substrates [26], a phenomenon observable at 48h[27]. It is inferred that the increased surface area allows for stable cellular adhesion, which is a prerequisite for cell cycle progression and proliferation[28]. Furthermore, micropatterns also affected cellular growth and alignment

when fibroblasts are confluent, thereby showing faster cellular alignment at the tissue level by synergistically interplaying with surface topography. Therefore, the highly aligned morphology at the tissue level observed in patterned hydrogels may be attributed to contact guidance-mediated interaction of the fibroblasts with the topographies. Thus, taken together the confocal fluorescence imaging and analysis of orientation results have revealed that the fibroblasts undergo contact guidance mediated alignment and growth process on the surface of the patterned hydrogels.

### 4. Conclusion

Here, we report a new cost-effective, and versatile method based on 3D printing that generates custom-made topographies on different acrylate hydrogels. The results demonstrated the ability of this novel 3D printed 24 well plate-sized PLA mold to efficiently engineer square topographies on different acrylated hydrogel surfaces such as HAMA, GelMA and PEGDA. Dermal fibroblast cell attachment studies showed the contact guidance potential of the patterned Hyaluronic acid hydrogel. The development of this type of new 3D PLA template with size compatibility of tissue culture plates can generate many stable surface patterned hydrogel samples with consistency and low cost. Guiding dermal fibroblasts on hydrogel surfaces holds significant promise for biomedical applications, particularly in wound healing research which includes the study of fibroblast recruitment to wound sites, extracellular matrix (ECM) molecule production, and the transition of fibroblasts to myofibroblasts in future studies. These characteristics may impact different fields of application in biomedical engineering such as tissue engineering, wound healing, mechanobiology, and disease modeling.

## 5. Acknowledgments

- This research work was supported by the Center for Engineering Mechanobiology (CEMB) grant
- 444 (CMMI-1548571) and CREST HBCU RISE grant (2332041) from the National Science
- Foundation. The authors thank Mr. Renjith Rajan Pillai (Graduate Researcher, UAB) for Keyence
- 446 Microscopy Imaging. VMV also thanks the faculty research award from Alabama State University.

## 6. Declaration of Competing Interest

The authors declare no competing financial interest.

#### 7. References

- 450 [1] E.M. Ahmed, Hydrogel: Preparation, characterization, and applications: A review, J Adv Res, 6 (2015)
- 451 105-121.

447

- 452 [2] T.C. Ho, C.C. Chang, H.P. Chan, T.W. Chung, C.W. Shu, K.P. Chuang, T.H. Duh, M.H. Yang, Y.C. Tyan,
- 453 Hydrogels: Properties and Applications in Biomedicine, Molecules, 27 (2022).
- 454 [3] A. Yasin, Y. Ren, J. Li, Y. Sheng, C. Cao, K. Zhang, Advances in Hyaluronic Acid for Biomedical
- 455 Applications, Front Bioeng Biotechnol, 10 (2022) 910290.
- 456 [4] Y. Piao, H. You, T. Xu, H.-P. Bei, I.Z. Piwko, Y.Y. Kwan, X. Zhao, Biomedical applications of gelatin
- 457 methacryloyl hydrogels, Engineered Regeneration, 2 (2021) 47-56.
- 458 [5] J.R. Choi, K.W. Yong, J.Y. Choi, A.C. Cowie, Recent advances in photo-crosslinkable hydrogels for
- 459 biomedical applications, BioTechniques, 66 (2019) 40-53.
- 460 [6] Y. Zhang, Y. Huang, Rational Design of Smart Hydrogels for Biomedical Applications, Frontiers in
- 461 Chemistry, 8 (2021).
- 462 [7] L. Cui, Y. Yao, E.K.F. Yim, The effects of surface topography modification on hydrogel properties, APL
- 463 Bioeng, 5 (2021) 031509.
- 464 [8] M. Ventre, P.A. Netti, Controlling Cell Functions and Fate with Surfaces and Hydrogels: The Role of
- 465 Material Features in Cell Adhesion and Signal Transduction, Gels, 2 (2016) 12.
- 466 [9] C. Leclech, C. Villard, Cellular and Subcellular Contact Guidance on Microfabricated Substrates,
- 467 Frontiers in Bioengineering and Biotechnology, 8 (2020).
- 468 [10] M.S. Hahn, L.J. Taite, J.J. Moon, M.C. Rowland, K.A. Ruffino, J.L. West, Photolithographic patterning
- of polyethylene glycol hydrogels, Biomaterials, 27 (2006) 2519-2524.
- 470 [11] M.F.A. Cutiongco, S.H. Goh, R. Aid-Launais, C. Le Visage, H.Y. Low, E.K.F. Yim, Planar and tubular
- 471 patterning of micro and nano-topographies on poly(vinyl alcohol) hydrogel for improved endothelial cell
- 472 responses, Biomaterials, 84 (2016) 184-195.
- 473 [12] S. Lv, J. Nie, Q. Gao, C. Xie, L. Zhou, J. Qiu, J. Fu, X. Zhao, Y. He, Micro/nanofabrication of brittle
- 474 hydrogels using 3D printed soft ultrafine fiber molds for damage-free demolding, Biofabrication, 12
- 475 (2020) 025015.
- 476 [13] H. Lai, B. Gong, J. Yin, J. Qian, 3D printing topographic cues for cell contact guidance: A review,
- 477 Materials & Design, 218 (2022) 110663.
- 478 [14] T.D. Clemons, M. Bradshaw, P. Toshniwal, N. Chaudhari, A.W. Stevenson, J. Lynch, M.W. Fear, F.M.
- 479 Wood, K.S. Iyer, Coherency image analysis to quantify collagen architecture: implications in scar
- 480 assessment, RSC Advances, 8 (2018) 9661-9669.

- 481 [15] F. Afghah, M. Ullah, J. Seyyed Monfared Zanjani, P. Akkus Sut, O. Sen, M. Emanet, B. Saner Okan, M.
- 482 Culha, Y. Menceloglu, M. Yildiz, B. Koc, 3D printing of silver-doped polycaprolactone-poly(propylene
- 483 succinate) composite scaffolds for skin tissue engineering, Biomedical Materials, 15 (2020) 035015.
- 484 [16] X. Tang, Y. Qin, X. Xu, D. Guo, W. Ye, W. Wu, R. Li, Fabrication and <i>In Vitro</i>
- 485 Printed Porous Polyetherimide Scaffolds for Bone Tissue Engineering, BioMed Research International,
- 486 2019 (2019) 2076138.
- 487 [17] V. Fitzpatrick, Z. Martín-Moldes, A. Deck, R. Torres-Sanchez, A. Valat, D. Cairns, C. Li, D.L. Kaplan,
- 488 Functionalized 3D-printed silk-hydroxyapatite scaffolds for enhanced bone regeneration with innervation
- and vascularization, Biomaterials, 276 (2021) 120995.
- 490 [18] J. Liu, C. Su, Y. Chen, S. Tian, C. Lu, W. Huang, Q. Lv, Current Understanding of the Applications of
- 491 Photocrosslinked Hydrogels in Biomedical Engineering, Gels, 8 (2022).
- 492 [19] A. Ansari, R. Trehan, C. Watson, S. Senyo, Increasing Silicone Mold Longevity: A Review of Surface
- 493 Modification Techniques for PDMS-PDMS Double Casting, Soft Mater, 19 (2021) 388-399.
- 494 [20] O. Ursini, M. Grieco, C. Sappino, A.L. Capodilupo, S.M. Giannitelli, E. Mauri, A. Bucciarelli, C.
- 495 Coricciati, V. de Turris, G. Gigli, L. Moroni, B. Cortese, Modulation of Methacrylated Hyaluronic Acid
- 496 Hydrogels Enables Their Use as 3D Cultured Model, Gels, 9 (2023).
- 497 [21] J. Chen, Z. Wang, J. Sun, R. Zhou, L. Guo, H. Zhang, D. Liu, M. Rong, K.K. Ostrikov, Plasma-Activated
- 498 Hydrogels for Microbial Disinfection, Adv Sci (Weinh), 10 (2023) e2207407.
- 499 [22] M.E. Smithmyer, L.A. Sawicki, A.M. Kloxin, Hydrogel scaffolds as in vitro models to study fibroblast
- activation in wound healing and disease, Biomater Sci, 2 (2014) 634-650.
- 501 [23] J. Lee, A.A. Abdeen, K.L. Wycislo, T.M. Fan, K.A. Kilian, Interfacial geometry dictates cancer cell
- tumorigenicity, Nature Materials, 15 (2016) 856-862.
- 503 [24] W. Yang, Y. qin, Z. Wang, T. Yu, Y. Chen, Z. Ge, Recent advance in cell patterning techniques:
- Approaches, applications and future prospects, Sensors and Actuators A: Physical, 333 (2022) 113229.
- 505 [25] S. Shivani, Y.-H. Hsu, C.-J. Lee, C.-S. Cheong, T.-T. Chung, A.-B. Wang, Programmed Topographic
- 506 Substrates for Studying Roughness Gradient-Dependent Cell Migration Using Two-Photon
- 507 Polymerization, Frontiers in Cell and Developmental Biology, 10 (2022).
- 508 [26] B. Majhy, P. Priyadarshini, A.K. Sen, Effect of surface energy and roughness on cell adhesion and
- 509 growth facile surface modification for enhanced cell culture, RSC Advances, 11 (2021) 15467-15476.
- 510 [27] A. Zareidoost, M. Yousefpour, B. Ghaseme, A. Amanzadeh, The relationship of surface roughness
- and cell response of chemical surface modification of titanium, J Mater Sci Mater Med, 23 (2012) 1479-
- 512 1488.

- [28] Q. Zhang, S. Lin, Q. Li, D. Zhao, X. Cai, Cellular Response to Surface Topography and Substrate
- 514 Stiffness, in: Y. Lin (Ed.) Cartilage Regeneration, Springer International Publishing, Cham, 2017, pp. 41-57.

- 1 3D Printing Assisted Surface Patterning Process on Acrylated Hydrogels for
- 2 Contact Guidance of Fibroblasts.
- 3 Amrita Natarajan<sup>#1</sup>, Suntae Kim<sup>#2,3</sup>, Gerardo Hernandez Moreno<sup>4</sup>, Jeroen Eyckmans<sup>2,3</sup>,
- 4 Christopher Chen<sup>2,3</sup>, Derrick Dean<sup>1</sup>, Vineeth M Vijayan<sup>1</sup>\*
- 5 <sup>1</sup>Laboratory for Polymeric Biomaterials, Department of Biomedical Engineering, Alabama State
- 6 University, Montgomery, AL 36104, USA
- 7 <sup>2</sup>Wyss Institute for Biologically Inspired Engineering, Harvard University, Boston, MA 02115,
- 8 USA
- 9 <sup>3</sup>Tissue Microfabrication Laboratory, Department of Biomedical Engineering, Boston University,
- 10 Boston, MA 02215, USA
- <sup>4</sup> Southern Research, Birmingham, AL 35294, USA.
- 12 # These authors contributed equally,
- \*Corresponding Author Email: vviijayan@alasu.edu
- 14 Abstract: Generating stable and customizable topography on hydrogel surfaces with contact
- 15 guidance potential is critical as it can direct/influence cell growth. This necessitates the
- 16 development of new techniques for surface patterning of the hydrogels. We report on the design
- of a square grid template for surface patterning hydrogels. The template was 3-D printed and has
- the diameter of a well in a 24-well plate. Hyaluronic acid methacrylate (HA) hydrogel precursor
- 19 solutions were cast on the 3D printed template's surface, which generated 3D square shape
- 20 topographies on the HA hydrogel surface upon demolding. The 3D Laser Microscopy has shown
- 21 the formation of a periodic array of 3D topographies on hydrogel surfaces. 3D Laser and Electron
- 22 Microscopy Imaging have revealed that this new method has increased the surface area and
- 23 exposed the underlying pore structure of the HA hydrogels. To demonstrate the method's
- 24 versatility, we have successfully applied this technique to generate 3D topography on two more
- 25 acrylate hydrogel formulations, gelatin Methacrylate and polyethylene glycol dimethacrylate.
- Human neonatal dermal fibroblast cells were used as a model cell line to evaluate the cell guidance

- 27 potential of patterned HA hydrogel. Confocal fluorescence microscopy imaging has revealed that
- 28 the 3D surface topographies on HA hydrogels can guide and align the actin filaments of the
- 29 fibroblasts presumably due to the contact guidance mechanism. The newly developed
- 30 methodology of 3D topography generation in acrylate hydrogels may influence the cell responses
- 31 on hydrogel surfaces which can impact biomedical applications such as tissue engineering, wound
- 32 healing, and disease modeling.
- 33 Total Word Count- 6363
- 34 Total Figures-8

Keywords: Hydrogels, Surface Patterning, Contact Guidance, Tissue Engineering

#### 1. Introduction

Hydrogels are three-dimensional crosslinked networks of polymers that can retain a large amount of water[1]. They are used for several biomedical applications such as drug delivery, tissue engineering, and wound healing[2]. Hydrogels formed from acrylate derivatives of polymers such as Hyaluronic acid Methacrylate[3], Gelatin Methacrylate[4], and Polyethylene Glycol Diacrylate[5] have received wide attention. This is mainly due to the acrylate bonds of natural and synthetic versions that can be crosslinked via photochemical or chemical strategies [5]. Acrylated hydrogels have wide utility for various biomedical applications such as bioink materials for 3D bioprinting, injectable scaffolds for tissue engineering, implantable drug delivery devices, and skin patches for wound healing[5, 6].

Hydrogel surface properties are critical for guiding cellular responses[7]. Most often, surface properties of the hydrogels such as surface roughness, surface area, and surface topography can impact/guide the cell responses[8]. Among the different surface cues, topography can play a major role in guiding cell responses[7]. This is mainly accomplished via contact guidance mechanisms. In the contact guidance process, cells receive active guidance signals from topographic cues such as grooves, ridges, or nano/micro patterns[9]. This impacts the different cell functions including proliferation, differentiation, and polarization[9].

Generating stable and customizable topography on hydrogel surfaces with contact guidance potential is very challenging and an area that needs active research[7]. Existing approaches for surface modification on hydrogels include but are not limited to photolithography[10], nanoimprint lithography[11], casting method[12], and 3D printing[13]. These methods have advantages and disadvantages. The lithographic technique, a common patterning method, requires a photomask that is not easily customizable and is not a cost-effective method[7]. Emerging methods like 3D printing show promise as they can print patterned hydrogels using computer-aided (CAD) software[13]. However, it is limited to only a few hydrogel formulations that meet the requirements of 3D printing. The casting method is one of the simplest and most effective methods to generate topographical patterns on hydrogel surfaces. Although a simple and effective method, this approach typically uses silicone molds which are not easily customizable. Also, there is a risk of the collapsing formed patterns due to excessive strains experienced by the mold material during the demolding process[7]. So a careful review of the literature shows that some of the existing challenges related to the generation of surface topography on hydrogel surfaces are (i) lack of customized templates/molds for generating the topographies, (ii) expensive nature associated with techniques such as photolithography, (iii) availability of very limited hydrogel formulations meeting the requirements of 3D printing, (iv) the stability issues of the patterns generated through simple techniques such as casting method and (v) finally the lack of scalability associated with these process. This very clearly suggests the importance of developing new surface topography generation processes on hydrogels that are simple, cost-effective, versatile, and scalable.

53

54

55

56

57

58

59

60

61

62

63

64

65

66

67

68

69

70

71

72

73

74

75

Inspired by these existing challenges associated with the generation of surface topographies on hydrogels, here we report a new method to generate 3D surface topography on hydrogels which

- is simple, cost-effective, and versatile. We have designed and 3D printed a 24-well plate-sized
- square-shaped Polylactic Acid (PLA) design. Up on casting with acrylated hydrogels such as HA,
- 78 GelMA and PEGDA has generated stable 3D surface topographies using this 3D printed PLA
- 79 template.

#### 2. Materials and Methods

- 81 Methacrylated hayluronic acid (HAMA), polyethylene glycol diacrylate (PEGDA), gelatin
- 82 methacrylate (GELMA), 2-hydroxy methacrylate (HEMA), ammonium persulfate (APS) and
- 83 ascorbic acid were purchased from Fischer Scientific. The polylactic acid (PLA) spool used for
- the 3D printing process was purchased from Flash Forge, United States.

## 85 <u>2.1. Design of the 3D Printed PLA Template</u>

- 86 Design requirements were formulated using an iterative approach with development being focused
- on compatibility with a 24-well plate design using SolidWorks software. A Flash Forge Creator
- 88 Max Dual Extruder 3D Printer was used for all 3D printing processes. 3D printing was done using
- 89 1.75 mm Poly (lactic acid) filaments. The printing temperature was set to 200° C and the print bed
- 90 was set at 50° C. A travel speed of 60 mm/s along with a print speed of 30 mm/s was used.

### 91 2.2. Preparation of Hydrogel Precursor Solutions

- 92 Initially, 10 mg HAMA was dissolved in 10 ml of dPBS solution (concentration of 1mg/ml) to
- 93 prepare the HAMA precursor solution for the hydrogel preparation. The initiator for the hydrogel
- 94 crosslinking Ammonium Persulfate (0.1M) was prepared by dissolving 114 mg of APS in 1 ml
- 95 dPBS solution (with a PH of 7.4). The catalyst for the crosslinking reaction Ascorbic Acid (0.1M)
- 96 was prepared by dissolving 88 mg of Ascorbic acid in 1 ml dPBS solution.

# 2.3. Preparation of Non-Patterned Hyaluronic Acid (HA) Hydrogel

The non-patterned HA hydrogels were prepared on a 24-well plate. Briefly, 400µl of hyaluronic acid methacrylate (HAMA) was added into a well followed by the addition of 200µl of 2-hydroxy ethyl methacrylate (HEMA) as the crosslinker. To initiate the free radical polymerization-induced crosslinking, 100µl of APS and Ascorbic acid were added quickly.

# 2.4. Preparation of Surface Patterned Hyaluronic Acid (HA) Hydrogel

To prepare the Surface patterned HA gel, we have placed the 3D-printed PLA mold inside the well of a 24-well plate. 400µl of Hyaluronic acid methacrylate (HAMA) was added on the top of the template followed by the addition of 200µl of 2-hydroxy ethyl methacrylate (HEMA). To initiate the free radical polymerization-induced crosslinking, 100µl of APS and Ascorbic acid were added quickly.

# 108 2.5. Preparation of Non-Patterned and Surface Patterned Gelatin Methacrylate (GelMA) and

# Polyethylene Glycol Diacrylate (PEGDA) Hydrogels

The non-patterned HA hydrogels were also prepared on a 24-well cell culture plate. Briefly,  $400\mu l$  of GelMA (1mg/ml stock solution) and PEGDA (3 mg/ml stock solution) were added into separate wells followed by the addition of  $200\mu l$  of 2-hydroxy ethyl methacrylate (HEMA) as the crosslinker. To initiate the free radical polymerization-induced crosslinking,  $100\mu l$  of APS and Ascorbic acid were added quickly.

The surface patterned GelMA and PEGDA hydrogels were formed using the same procedure with the difference of casting the solutions over the 3D printed PLA template to generate surface topography.

# 118 2.6. Characterization of the Hydrogels 119 The viscoelastic behavior of the hydrogels was measured using a TA Instruments Discovery HR-120 2 Rheometer. The surface features of surface patterned& non-patterned HA gels were studied using 121 3D Laser Scanning Confocal Microscope VK-X1000. The surface areas of the surface patterned, 122 and non-patterned hydrogels were measured using VK-X3000 3D Surface Profiler feature of the 123 Keyence Microscope. The surface topography of the hydrogels were performed using a Phenom 124 XL Benchtop Scanning Electron Microscope. 125 2.7. Plasma Surface Modification of the Hydrogels 126 The surface-patterned and non-patterned hydrogels were surface-modified using a Harrick Plasma chamber. More specifically, hydrogels were placed inside the chamber with an airflow rate of 20 127 128 sccm and subsequently, plasma was ignited after applying a radiofrequency of 13.56 MHz and 45 129 W for 5 minutes. 2.8. Cell culture 130 131 Human neonatal dermal fibroblast was purchased from Lonza(CC-2509). The fibroblast grew in 132 FGM<sup>TM</sup>-2 Fibroblast Growth Medium-2 BulletKit<sup>TM</sup>(Lonza, CC-3132) under 37°C, 95% 133 humidity, and 5% CO2 conditions. All the cells were used in passages 3-5 and the media was 134 replaced every other day. 135 2.8.1. Cell adhesion experiment on HA gels 136 Physical collagen coating on the hydrogels was conducted before seeding the fibroblasts. Fully 137 swollen HA gels were sterilized by emitting UV light for 15 minutes each on both sides. The sterile 138 hydrogels were placed into 24 well plates and soaked overnight at 4° C in 200 μg/ml collagen type

I solution (Corning, 356236) diluted with DI water. The hydrogels were washed with PBS 3 times right before seeding the fibroblasts. When the fibroblasts reached around 80% confluency, the cells were washed with PBS and enzymatically detached (0.05% trypsin/EDTA). 2x 10⁴ cells for low density and 1 × 10⁵ cells for high density were seeded in each well plate with 1ml of media. For actin staining and imaging, the hydrogels were fixed with 4% paraformaldehyde (Electron Microscopy Sciences, 15710) for 30 min at specific time points after seeding(3,6,24,48h). After blocking with 2% BSA in PBS for 1h at room temperature, Alexa Fluor™ Plus 555 Phalloidin(Thermofisher Scientific, A30106, 1:1000), and DAPI (Sigma, D9542, 1:1000) were incubated for 2h at room temperature. The samples were washed with PBS between each step. Confocal and 3D images were acquired with a Leica HC FLUOTAR L 10x and 40x water-immersion objective on an upright TCS SP8 multiphoton microscope (Leica)

# 2.8.2. Quantification of actin images by ImageJ

We quantified cell area, orientation coherency, and orientation distribution by using the "measure", "directionality" and "OrientationJ" plug-in in ImageJ as described previously[14]. Mean intensity and cell area were simply measured by the "measure" function after setting the scale for 40x image (n=20). For coherency and distribution analysis, all the actin images were rotated to match the most aligned actin filament to 0 degrees using the horizontal alignment function in Orientation J. Then, the "dominant direction" function in Orientation J was utilized to calculate orientation coherency from 0 (no alignment) to 1 (perfect alignment) (n=6). The orientation distribution data of actin can be obtained by the "directional" function with the Fourier component method.

## 2.9. Statistical Analysis

One-way ANOVA was conducted to analyze the differences between patterned and no pattern groups. For the group analysis over time, two-way ANOVA was employed to compare the mean values. From \*P < 0.05, it is considered to have statistical significance. (n.s., not significant, \*P < 0.05, \*\*P < 0.01, \*\*\*P <0.001, \*\*\*\*P<0.0001.) Statistical analyses were performed using GraphPad prism. All data points on the graphs represent average values, and error bars depict the SEM.

### 3. Results and Discussion

160

161

162

163

164

165

166

167

168

169

170

171

172

173

174

175

176

177

178

179

180

181

182

The major interest of this work was to develop a simple, cost-effective, and versatile method to generate 3D surface patterning method on hydrogel surfaces. 3D printing thermoplastic polymers like Polylactic Acid is one of the most cost-effective methods in additive manufacturing. Inspired by this, we decided to use a 3D-printed PLA template design to guide the generation of topographies on hydrogel surfaces. We hypothesized that the usage of a custom 3D printed mold for casting the hydrogel solutions would generate negative impressions of the positive mold material. To test this hypothesis, we have manufactured a 3D-printed square grid using a fused deposition modeling technique using PLA. The dimensions of the 3D design iterations were based on 24-well polystyrene plates used for cell culture. We first measured the dimensions of a 24-well plate and used that as a baseline to design the PLA template. The printed PLA construct has a diameter of 15 mm with each square in the grid pattern measuring 1mm fitting well within a 24well plate (Figure 1a). The rationale behind printing a 24-well plate size design was to generate surface-patterned hydrogels which can easily facilitate in vitro cell studies. Usually, to perform in vitro testing using biomaterials, researchers often need to cut or manipulate their material constructs to be used for cell culture well plates to allow for the proximity of the material to the cell monolayer[15]. Other groups grow their cell model on their respective materials and then are

required to detach the cells for analysis in separate dishes[16] or well plates[16, 17]. This is inconvenient and can be an issue related to time and material waste concerning critical cell-based assays for analysis of biocompatibility. Hence, designing surface patterned hydrogel that exactly fits the size of a cell culture well plates will be an efficient method to generate more reliable and consistent results with cell studies.

The confocal laser surface scanning microscopy showed a clear transfer of the mold pattern from the design to the printed structure (Figure 1b). The square grid-type pattern was observed from the images with closed cavities which can hold hydrogel solutions while casting (Figure 1c,d). Subsequently, we have used Methacrylated Hyaluronic Acid (HA) as the precursor for HA hydrogel formation. The experimental plan for generating the surface-patterned HA hydrogel using the casting method on the template/mold was shown schematically (Figure 1e). More specifically, hydrogel solution along with crosslinkers and initiator will be cast on the PLA template which forms a hydrogel and upon demolding would generate negative impressions of the positive mold material.

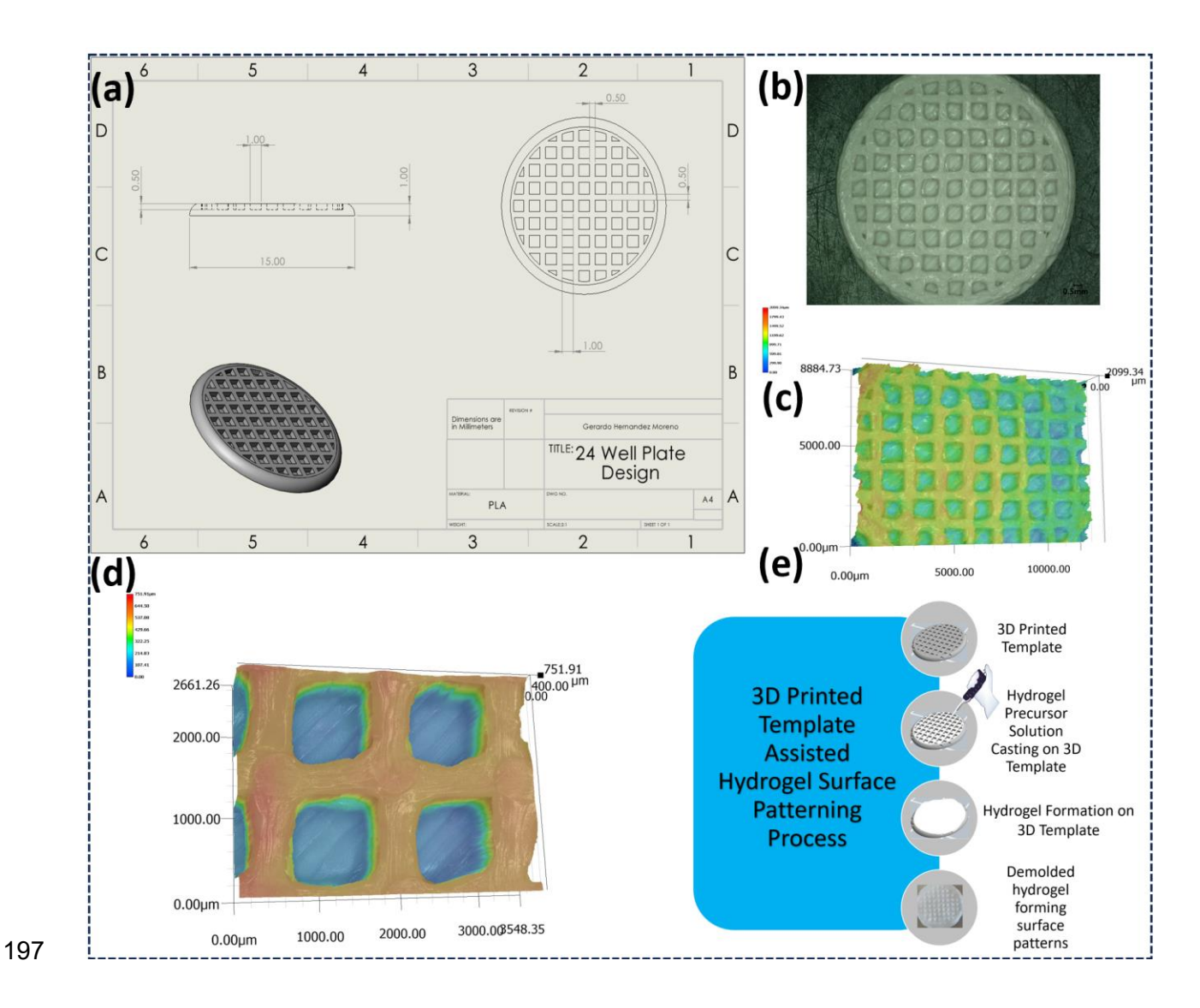


Figure 1: Design Iteration of the 24 well plate sized PLA template from SolidWorks Software (a), Laser Surface Scanning Microscopy Images of the 3D printed PLA template (b-d), 3D Laser Scanning Microscopy Images of the 3D, the schematics of the 3D printed template assisted process (e).

The hydrogel-forming solutions were poured on the mold and placed inside a 24-well plate. We have observed that with time there was a development of turbidity inside the wells which is an indication of the crosslinking process (Figure 2a). The mechanism of hydrogel formation was based on a free radical-initiated chemical crosslinking process. (Figure 2b). Specifically, the unsaturated double bonds of the methacrylated hyaluronic acid were crosslinked using another unsaturated vinyl monomer 2-Hydroxy ethyl methacrylate (HEMA) using a radical initiator

Ammonium Persulfate. The rationale behind using the free radical-initiated chemical crosslinking process was to generate hydrogels with strong mechanical properties. Conventionally in the surface patterning process, researchers use photo crosslinking of methacrylated polymers such as HA, GelMA, and PEGDA which is found to provide weaker mechanical properties to the resultant hydrogels[18]. So, we anticipated that the strong chemical crosslinking process will provide the necessary strength to our hydrogels which can withstand the stress associated with the demolding process without collapsing the patterns.

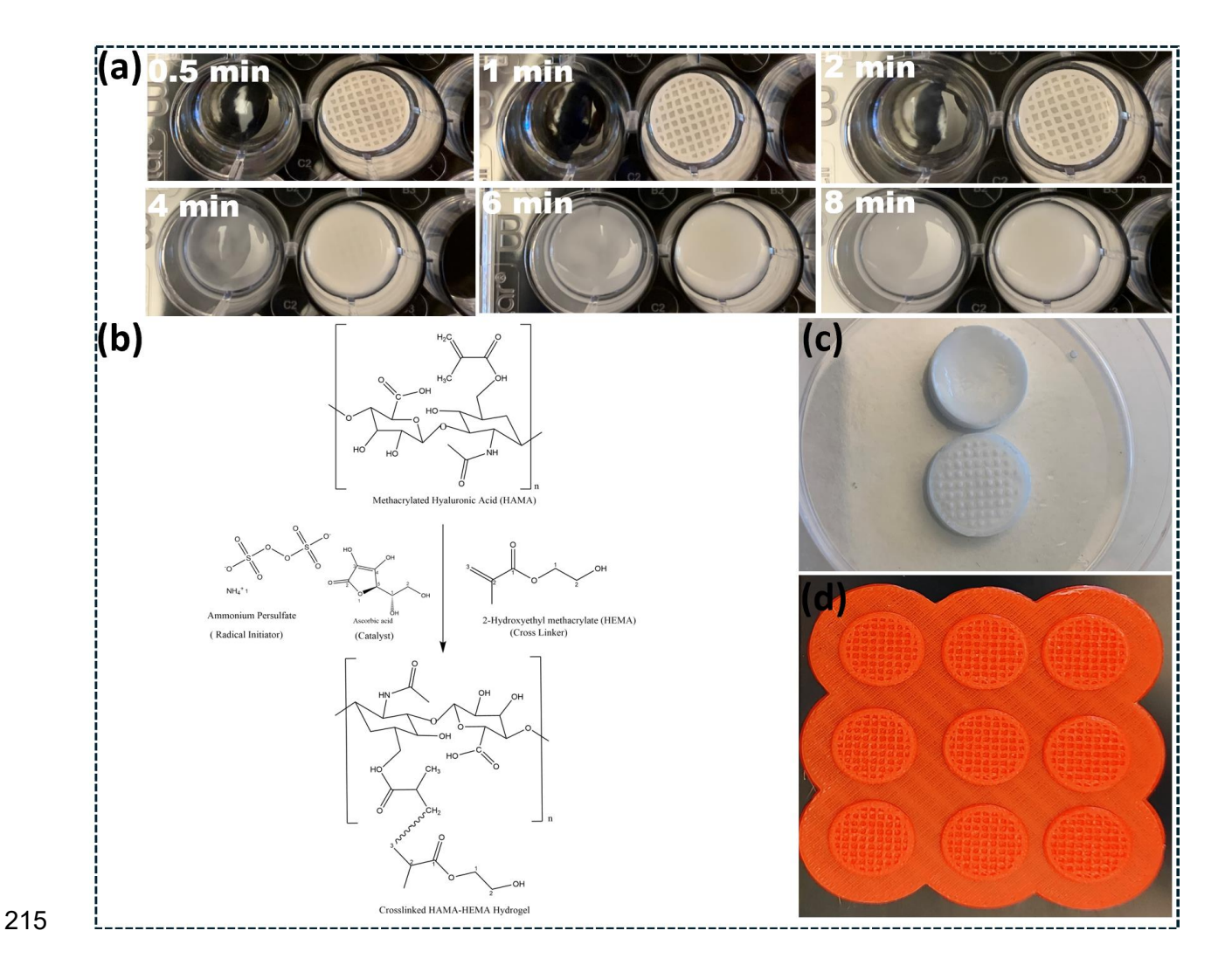


Figure 2: The images showing the comparison of the hydrogel formation on the plain 24-well plate and the top of the 3D template at different time points (a), the chemical crosslinking process of the Hyaluronic Methacrylate and 2-Hydroxy Ethyl Methacrylate forming the HA hydrogel (b), the

photographs of the non-patterned and patterned hydrogels after the crosslinking process (c), image of the nine 3D printed PLA template structures (d).

219220

221

222

223

224

225

226

227

228

229

230

231

232

233

234

235

236

237

238

239

240

241

242

After the crosslinking process, we carefully demolded/removed the hydrogel from the PLA mold resulting in the production of HA hydrogels with stable surface patterns which are the negative impressions from the positive mold material (Figure 2c). The scalability of the 3D printing was demonstrated by printing 9 designs together with consistency (Figure 2d). This is another advantage of this process compared to PDMS-based molds in photolithography which are not easily customizable and scalable for surface patterning[19].

The FTIR spectra comparison has shown a decrease in the C=C stretching peak (1645 cm<sup>-1</sup> 1) intensity for the final crosslinked hydrogel in comparison with the HA and HEMA, this suggested the chemical crosslinking process of double bonds during hydrogel formation (Figure S1). Next, we have performed rheology measurements to identify important parameters such as the stiffness and the gelation time of the hydrogels. Time sweep experiments have shown that at 375 seconds the gelation process starts occurring which was evident by the increase in complex viscosity and cross-over between the storage and loss modulus of the hydrogels (Figure 3a). The frequency sweep experiments of the HA hydrogels were conducted to measure the storage modulus of the hydrogels. The results of the frequency seep experiment have demonstrated a higher storage modulus value of 1000 kPa for the HA hydrogel (Figure 3b). Generally, the Hyaluronic Acid Methacrylate is photo-crosslinked using initiators like Irgacure to produce HA hydrogels. However, the storage modulus of these photo-crosslinked HA hydrogels is relatively weak in the range of 10-100 Pa [20]. However, our present chemically crosslinked HA hydrogel displayed a very high storage modulus value which was several folds higher than the conventional photocrosslinked HA hydrogel formulations. This observed significant increase in the strength of the prepared HA hydrogel can be attributed to the strong chemical crosslinking process. This high

stiffness of the HA hydrogels supports the generated topographies and provides stability to the formed patterns without collapsing after the demolding process from the PLA template.

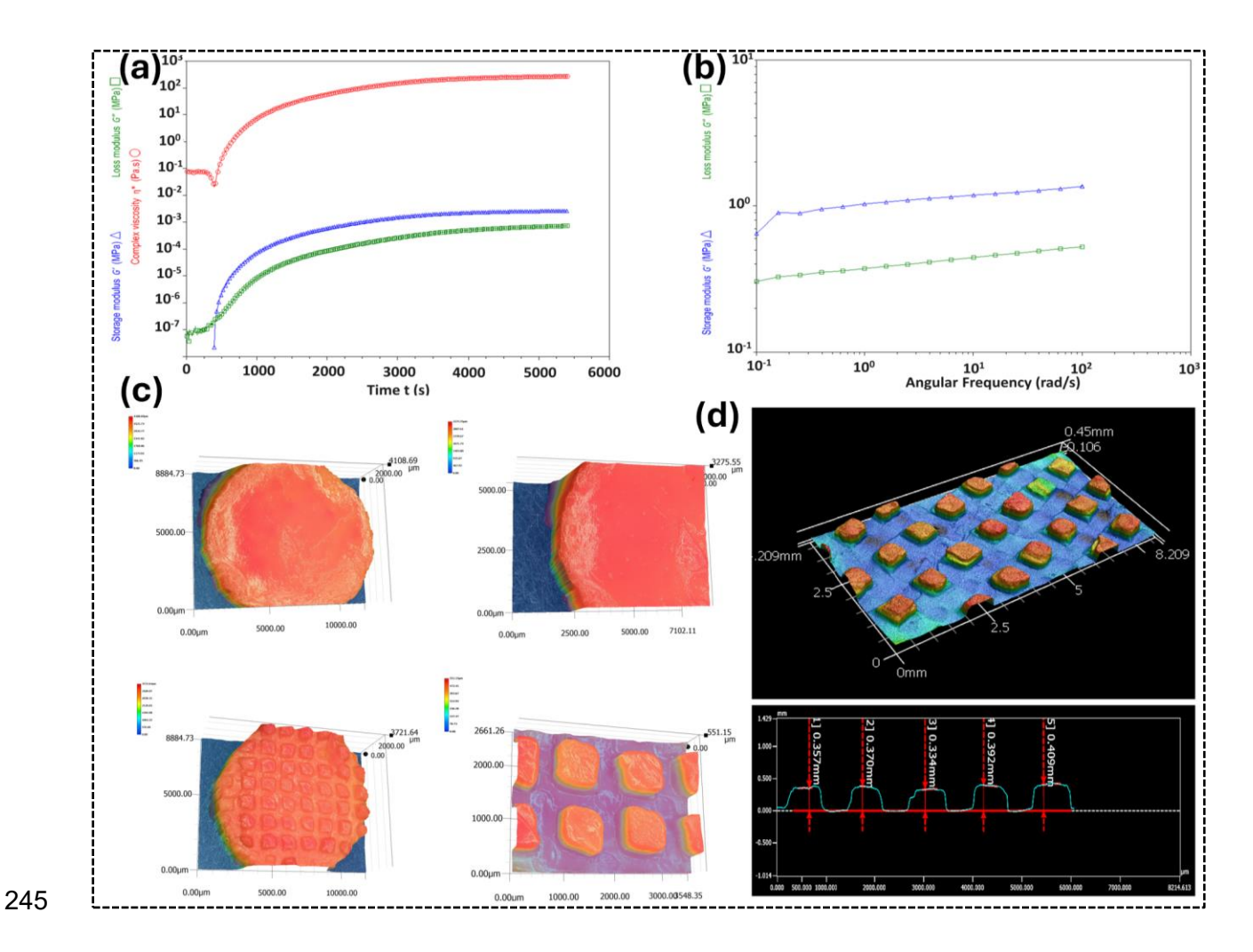


Figure 3: Rheological Measurements of HA hydrogels, time sweep experiments(a), frequency sweep experiments (b). 3D Laser Scanning Microscopy Images of the patterned and non-patterned hydrogels (to increase the contrast of the image food color dye was added on the hydrogel before taking the images) (c), Images showing the quantification of the width and height/depth of the square patterns formed on the surface of the HA hydrogels using the surface profiling measurements (d).

Images from the 3D laser confocal microscopy showed the periodic 3D array of square-shaped topographical patterns formed on the hydrogel surface (Figure 3c). More specifically, the surface of the hydrogel was composed of square-shaped pillars with periodic interspacing between the pillars throughout the entire surface of the HA hydrogel. The average surface area of the HA

hydrogel was measured using the surface profiling feature of the 3D laser confocal scanning microscopy by selecting 17 different spots on the patterned hydrogel (Figure S2). The average surface area of the patterned hydrogel was found to be 0.760 mm<sup>2</sup>. In the case of un-patterned hydrogel surface, a completely flat surface topography was observed with an average surface area of 0.007 mm<sup>2</sup>. Thus, it was clear that the 3D printed patterned molds introduced surface patterning and increased the overall surface area of the HA hydrogel. The 3D surface profiling of the hydrogels showed the average height and width of the square pillars to be 311 and 870µm (Figure 3d). The actual 24-well plate PLA template/mold has a depth of 500 µm and a pore width of 1000 um. Hence, the expected height and width of the square patterns formed on the hydrogel surface should be around 500 and 1000 µm. However, the observed height and width of the square patterns (311 and 870µm) were lower than these values. This difference may be attributed to the printing resolution issues with the 3D printer. Improving the printing resolution may create a closer alignment in the height and width of the square patterns in the design and hydrogel constructs. The reported observations corroborated our initial hypothesis by printing 2 more additional PLA templates with pore widths of 2000 and 3000 µm. Casted HA hydrogels were poured on its surface and subsequently demolded. As the pore width of the template increased the uniformity of the square shape generated on the hydrogel surface significantly improved (Figure S4). This observation suggested that printing low pore width templates is challenging and needs more systematic optimization of printing parameters such as print speed, nozzle diameter and nozzle temperature. As low size and higher number of surface patterns are critical for governing the cell response such as those that arise from increased surface area, we have chosen the 1000 µm template mold patterned hydrogels for further studies.

256

257

258

259

260

261

262

263

264

265

266

267

268

269

270

271

272

273

274

275

276

Subsequently, we have taken the Scanning Electron Microscopy images of the patterned vs non-patterned HA hydrogels. Interestingly, it was seen that the hydrogels with the 3D surface topography exposed the underlying porosity than the non-patterned ones (Figure 4). This difference in the pore structure could be attributed to the square cavity structures of the PLA mold. More specifically, on the flat 24-well plate surface, the hydrogel precursor solutions (the polymer, crosslinker, initiator, and catalyst solutions) form a continuous film whereas inside the mold there is a non-continuous and confined distribution of hydrogel precursors are present which can impact the formation of hydrogels on the template.

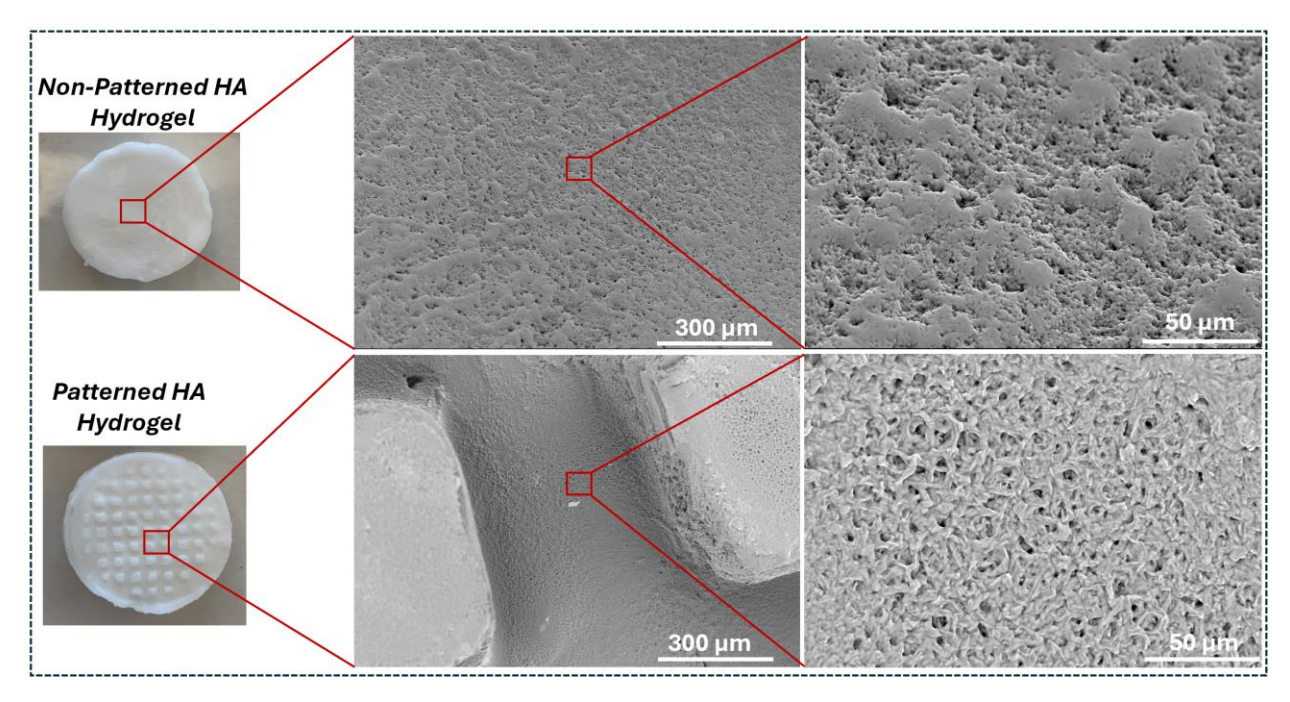


Figure 4: The Scanning Electron Microscopy Images showing the topography and pore structure of Hyaluronic Acid Methacrylate Hydrogels formed on the flat 24 well plate versus 3D printed PLA template surface

We speculate that the formation of hydrogel on the template will be impacted by the hydrostatic pressure caused by the square-shaped cavities of the mold. This is because each square cavity of the PLA mold has an average depth of 650µm (Figure S3). This may contribute towards the generation of hydrostatic pressure on the hydrogel precursor solutions proportional to the

depth. Non-patterned hydrogels are formed by casting the hydrogel solution on a plain surface of the 24-well. More in-depth quantitative experiments are needed to validate this speculation and our future studies will attempt to address it. Hence, we believe that these factors of confined non-continuous distribution of the hydrogel-forming solutions and the possibility of experiencing hydrostatic pressure on the templates could have impacted the pore structure of the hydrogels in comparison with hydrogels formed on the flat 24-well plate surface. This shows the positive impact of the template material on exposing the pore structure of the hydrogel.

Method versatility was shown by applying the same 3D printed mold to other methacrylate hydrogel-forming materials Gelatin Methacrylate (GelMA) and Polyethylene Glycol Diacrylate (Figure S5). The SEM images of the patterned hydrogels of both GelMA and PEGDA showed the clear formation of a square pattern with more exposed pores compared to non-patterned ones. This observation supports the role of hydrostatic pressure on the pore structure of the hydrogel regardless of its composition. To assess the capability of the 3D topographies generated on the hydrogel surfaces, we have conducted cell attachment studies on HA hydrogels.

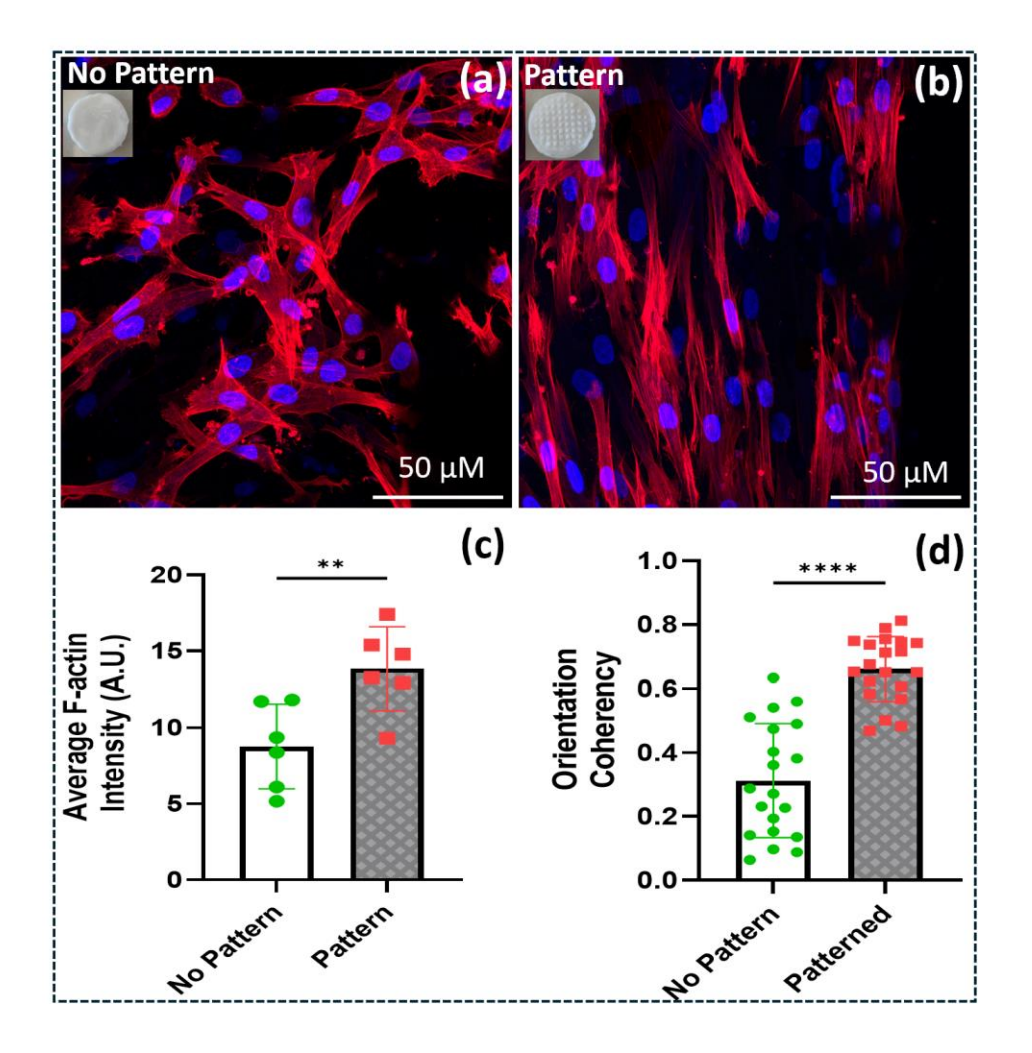


Figure 5. Fluorescent visualization of fibroblast of low density on collagen-coated HA gel without and with a surface pattern (a, b). Fluorescence images of F-actin (red) and nuclei (blue) stained human dermal fibroblast at 2 hours. (scale bars represent 50  $\mu$ m for 40x). Analysis of F-actin intensity and orientation coherency of single cells measured with ImageJ. (c, d) 0 means no alignment and 1 is perfectly aligned Measurement and comparison of the change in cell (\*P < 0.05, \*\*P < 0.01, \*\*\*P < 0.001, \*\*\*\*P < 0.0001)

For the cell studies, HA hydrogels were fabricated using the square grid pattern and demolded to get the surface-patterned hydrogels. The PLA template used to generate the patterns was discarded immediately after the generation of the surface patterns and only surface-patterned HA hydrogel samples were used to conduct cell attachment studies. Prior to the cell attachment studies, hydrogels were subjected to plasma treatment[21] and collagen coating[22]. This was to provide sterilization and facilitate better fibroblast attachment. Initially, we used a low fibroblast

seeding density to study the effect of topography on cell attachment. Fluorescence microscopy images of fibroblasts on surface-patterned hydrogels at the 2-hour time point showed increased Factin intensity and alignment compared to control non-patterned hydrogels (Figure 5 a&b). To get more quantitative insight into the alignment process, we have measured the fluorescence intensity and orientation coherency of the F-Actin filaments at a single-cell level on patterned and nonpatterned hydrogels (Figure 5c&d). We have observed a higher orientation coherency at the initial time point for patterned hydrogels which was indicative of the alignment of F-Actin filaments on patterned hydrogel surface. It was seen that the F-Actin filaments and the nuclei of the cells were aligned in a vertical/horizontal direction. It is important to note that the hydrogels are patterned using a template having a grid pattern that has each individual square arranged identically in both vertical and horizontal directions with similar dimensions and spacing (Figure 1a&b). The SEM image of the patterned hydrogel shows the 2 adjacent square topographies formed in the horizontal direction showing the position and spacing of the topographies consistent with the grid template (figure 4). The low cell seeding density fluorescent images of the patterned surfaces showed an orientation of the F-Actin and nuclei of cells in a vertical/horizontal direction consistent with the directionality of the grid patterns of the template. As the squares are identical in both vertical and horizontal directions in the template, we believe that there will be an equal probability for orientation in vertical/horizontal directions.

321

322

323

324

325

326

327

328

329

330

331

332

333

334

335

336

337

338

339

340

341

342

343

The surface-patterned hydrogel has a significantly higher surface area (0.760 mm²) compared to the control non-patterned hydrogel (0.007 mm²) in 3D topography imaging (Fig S2), this result suggested hydrogel with a large surface area facilitates initial cell attachment. This effect is likely due to the larger surface area providing a higher density of functional groups that cells can recognize and bind to and facilitating mechanical interlocking between cells and substrate[23].

This enhances physical anchoring and stability, thereby improving cell-topography interactions through contact guidance.

344

345

346

347

348

349

350

351

352

353

354

355

356

357

358

359

360

361

Subsequently, we have also analyzed cellular growth at different time intervals such as 3, 6, 24, and 48h with high cell density (Figures 6a&b). Previously, we observed differences in initial cell attachment based on surface patterns. Further, this study was conducted to evaluate the longterm impact of cellular growth on the tissue-level orientation capabilities of the patterned hydrogels. The multiphoton confocal fluorescence images of the cytoskeleton and nuclei arrangement of the dermal fibroblasts (F-actin in red and cell nuclei in blue) cultured in the patterned and non-patterned hydrogels were qualitatively and quantitatively analyzed after 3h, 6h, 24h, and 48h. The patterned HA hydrogel surface consists of repeating square pillars with periodic interspacing. Notably, fibroblasts were confined to the flat grooves between the pillars. Confocal fluorescence imaging at 10x magnification showed fibroblasts forming a cross-like pattern within these grooves (Figure 6a). In contrast, fibroblast attachment on the control un-patterned hydrogel was random without any confinement. Hence, it was clear that the topography formed on the hydrogels provided a confined/closed growth pattern to hydrogels. This showed the impact of the topographies on fibroblast response. It was already reported that small-scale microtopography and patterning could impact the growth pattern of the cells [23, 24]. However, these low-magnification images do not show any orientation/alignment of the cells in the patterned hydrogels at 3 and 6h.

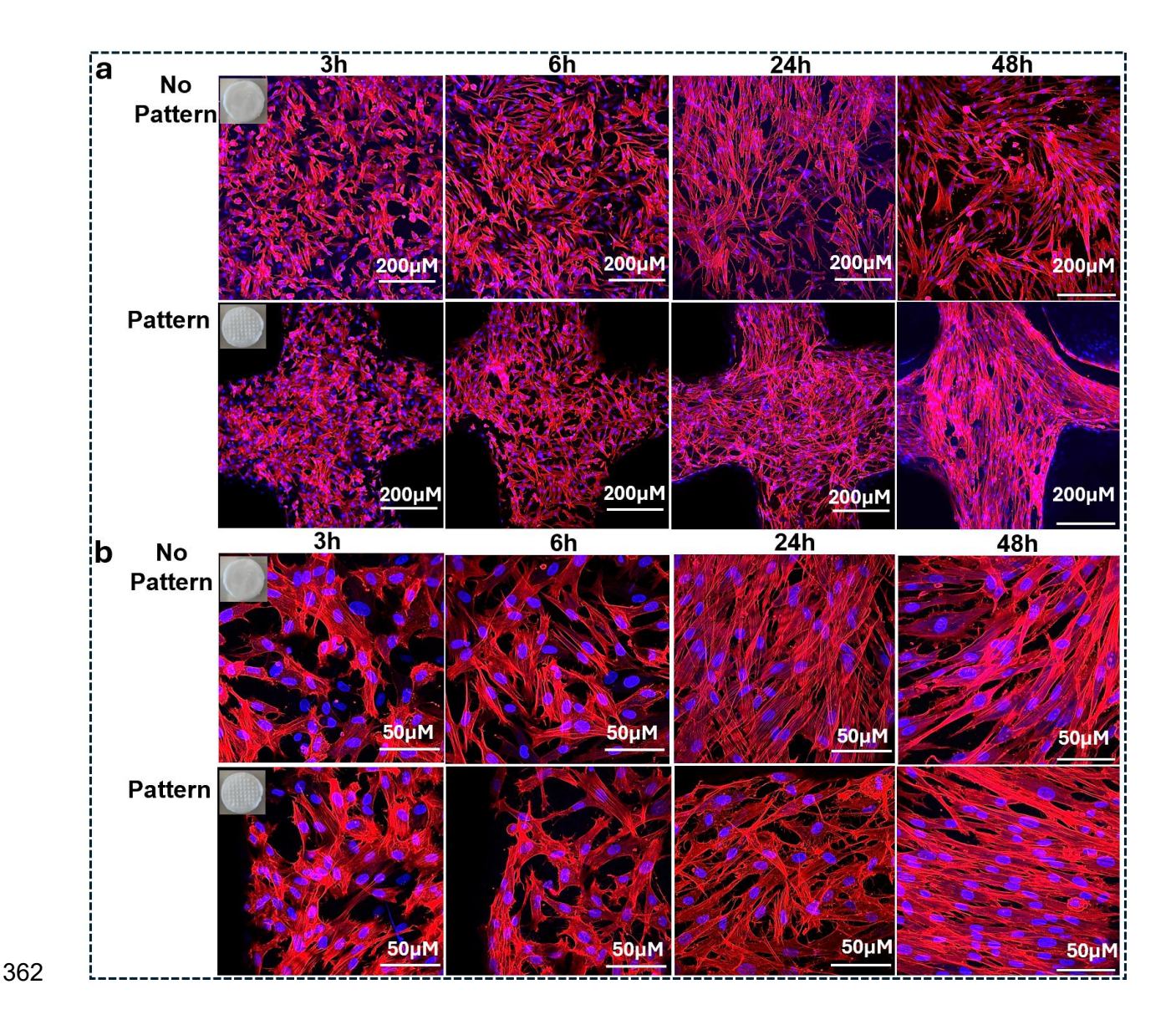


Figure 6: Fluorescent visualization of fibroblast of high density on collagen-coated HA gel with and without a surface pattern: Fluorescence images of F-actin (red) and nuclei (blue) stained human dermal fibroblast over time (1,2,3,6,24,48h) at 10 and 40X magnifications with and without a pattern (a, b).

The higher magnification confocal fluorescence microscopy images (40X) were taken and compared for both patterned and non-patterned hydrogels to examine the F-Actin orientation of fibroblasts grown on patterned and non-patterned hydrogels (Figure 6b). The quantitative orientation coherency calculation shows that the orientation of cells was not significant for both types of patterned and non-patterned hydrogels at early time points 3,6 and 24h (Figure 6a&b).

However, after 48h, there were significant disparities in the shape, morphology, and orientation of cultured cells within the patterned hydrogel was observed (Figure 6a&b).

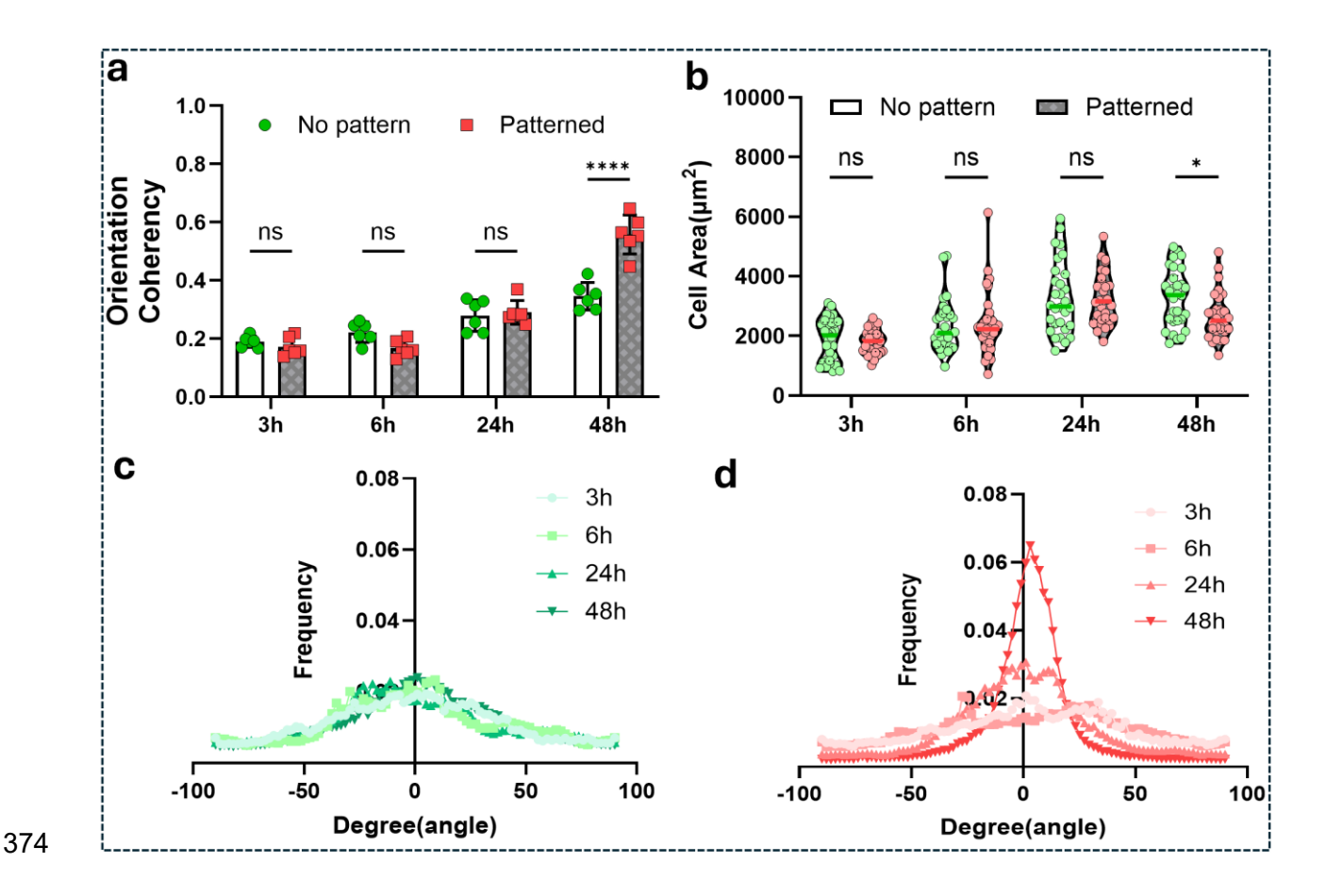


Figure 7: Analysis of orientation coherency calculated by directionality plug-in in ImageJ. 0 means no alignment and 1 is perfectly aligned (a), Measurement and comparison of the change in cell area over time for no pattern and patterned HA gel (b), Orientation distribution of stained F-actin on (c) no pattern and (d) pattered gels over time (n.s., not significant, \*P < 0.05, \*\*P < 0.01, \*\*\*P < 0.001, \*\*\*P < 0.0001).

More specifically, over time progression, there was an augmentation in the cell area up to 24h, attributed to cellular spreading and stable adhesion to the substrate. The cytoskeletal organization of cells on patterned hydrogel exhibited pronounced orientation coherency, particularly evident at the 48-hour time point in contrast to the non-patterned counterpart (Figure 7a). However, a reduction in cell area was observed specifically in the patterned hydrogel at 48h which cell alignment was actively observed (Figure 7b). Additionally, the frequency distribution graph

illustrated a distinct alignment pattern of actin filaments exclusively on the patterned hydrogel at 48h (Figure 7c, d).

The observed alignment of the fibroblasts on the patterned hydrogel at a longer time of 48h could be attributed to the increased cell-topography interaction and cell-cell interactions. More specifically, the observed confined growth of the cells through the grooves of the square patterns is expected to increase with time which can result in a more confined/narrow arrangement of cells. This was evident by the low magnification fluorescence image comparison of patterned and nonpatterned hydrogels at 3,6,24 and 48h (figure 6a). It was seen that the confined/narrow cell arrangement progressively increased with time and reached the maximum at 48h as evidenced by the most confined F-Actin and nuclei arrangement. Based on this observation, we believe that there is an increased topography-cell interaction at 48h. Also, it is very important to account for the high cell-cell interactions that may be present at a longer time point of 48h which can also contribute to the observed alignment process. Hence, we believe that there is a combinatory effect of topography-guided confined growth and increased cell-cell interactions which results in the observed alignment of the cells at 48h. More detailed investigations should be conducted to fully explore the exact mechanism behind this phenomenon and our future studies will aim to explore this.

Z stack confocal imaging was used to examine the three-dimensional distribution of cells on patterned hydrogels. At 48 hours, It was seen that cells displayed oriented intracellular actin filaments and aligned along the grooves of the patterned hydrogel-forming a cross-like pattern whereas for the non-patterned hydrogel, there was no observation of confined growth or alignment.

407 (Figure 8).

386

387

388

389

390

391

392

393

394

395

396

397

398

399

400

401

402

403

404

405

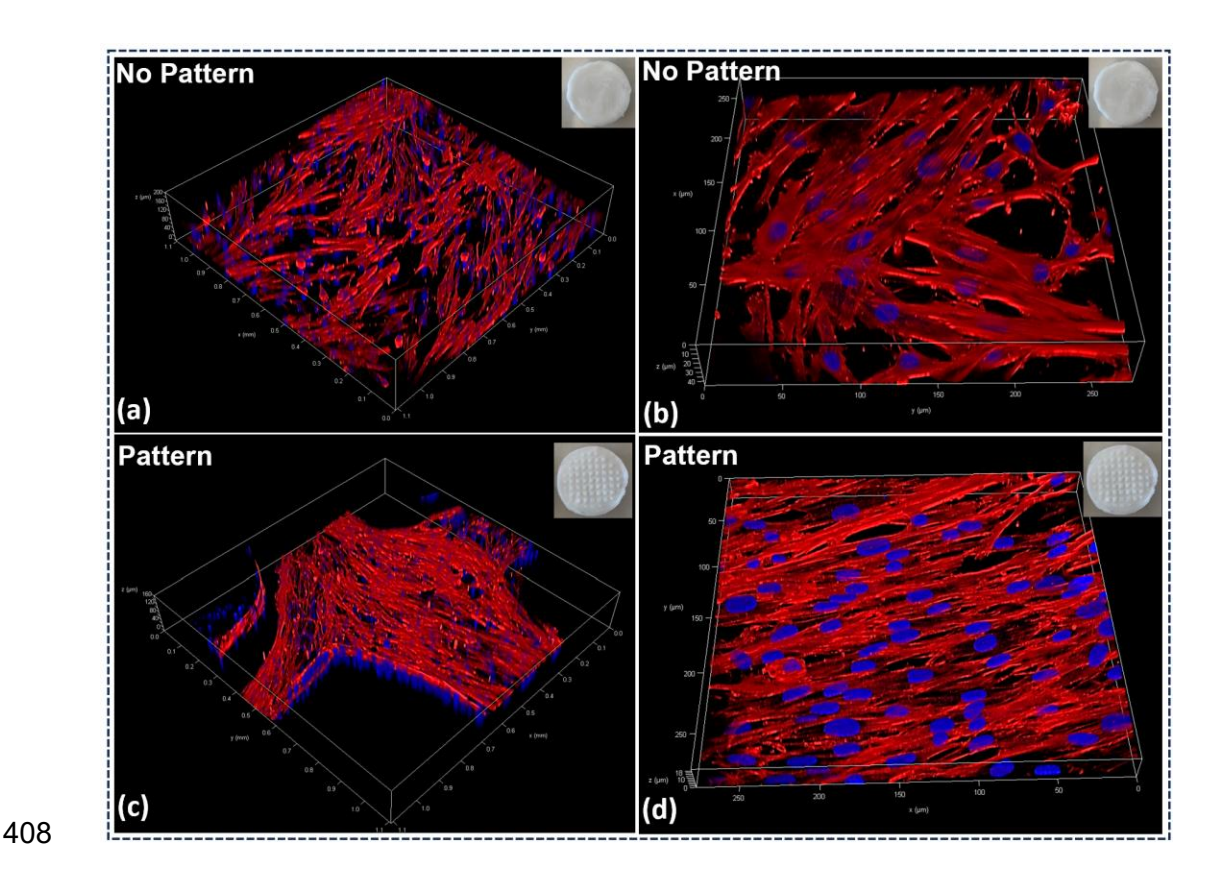


Figure 8: Z stack 3D Confocal Fluorescent images of the collagen-coated HA gel with and without a surface pattern. The images show F-actin (red) and nuclei (blue) stained human dermal fibroblast at 48h time points taken at different magnifications, 10X(a,c) and 40X (b,d).

These results indicate that a higher fibroblast density on patterned hydrogels facilitates a more rapid orientation of F-Actin filaments at the tissue level. Cellular alignment at the tissue level was not observed during the initial stages, likely due to the combined effects of intercellular and cell-substrate interactions under high-density conditions. However, as fibroblasts enter the proliferation stage over time, cellular alignment at the tissue level becomes clearly observable at 48 hours. It was previously reported that cells on substrates with porous and larger surface areas demonstrated increased migration velocity[25], and are more conducive to cell proliferation compared to flattened substrates [26], a phenomenon observable at 48h[27]. It is inferred that the increased surface area allows for stable cellular adhesion, which is a prerequisite for cell cycle progression and proliferation[28]. Furthermore, micropatterns also affected cellular growth and alignment

when fibroblasts are confluent, thereby showing faster cellular alignment at the tissue level by synergistically interplaying with surface topography. Therefore, the highly aligned morphology at the tissue level observed in patterned hydrogels may be attributed to contact guidance-mediated interaction of the fibroblasts with the topographies. Thus, taken together the confocal fluorescence imaging and analysis of orientation results have revealed that the fibroblasts undergo contact guidance mediated alignment and growth process on the surface of the patterned hydrogels.

## 4. Conclusion

Here, we report a new cost-effective, and versatile method based on 3D printing that generates custom-made topographies on different acrylate hydrogels. The results demonstrated the ability of this novel 3D printed 24 well plate-sized PLA mold to efficiently engineer square topographies on different acrylated hydrogel surfaces such as HAMA, GelMA and PEGDA. Dermal fibroblast cell attachment studies showed the contact guidance potential of the patterned Hyaluronic acid hydrogel. The development of this type of new 3D PLA template with size compatibility of tissue culture plates can generate many stable surface patterned hydrogel samples with consistency and low cost. Guiding dermal fibroblasts on hydrogel surfaces holds significant promise for biomedical applications, particularly in wound healing research which includes the study of fibroblast recruitment to wound sites, extracellular matrix (ECM) molecule production, and the transition of fibroblasts to myofibroblasts in future studies. These characteristics may impact different fields of application in biomedical engineering such as tissue engineering, wound healing, mechanobiology, and disease modeling.

## 5. Acknowledgments

- This research work was supported by the Center for Engineering Mechanobiology (CEMB) grant
- 444 (CMMI-1548571) and CREST HBCU RISE grant (2332041) from the National Science
- Foundation. The authors thank Mr. Renjith Rajan Pillai (Graduate Researcher, UAB) for Keyence
- 446 Microscopy Imaging. VMV also thanks the faculty research award from Alabama State University.

## 447 6. Declaration of Competing Interest

The authors declare no competing financial interest.

## 449 7. References

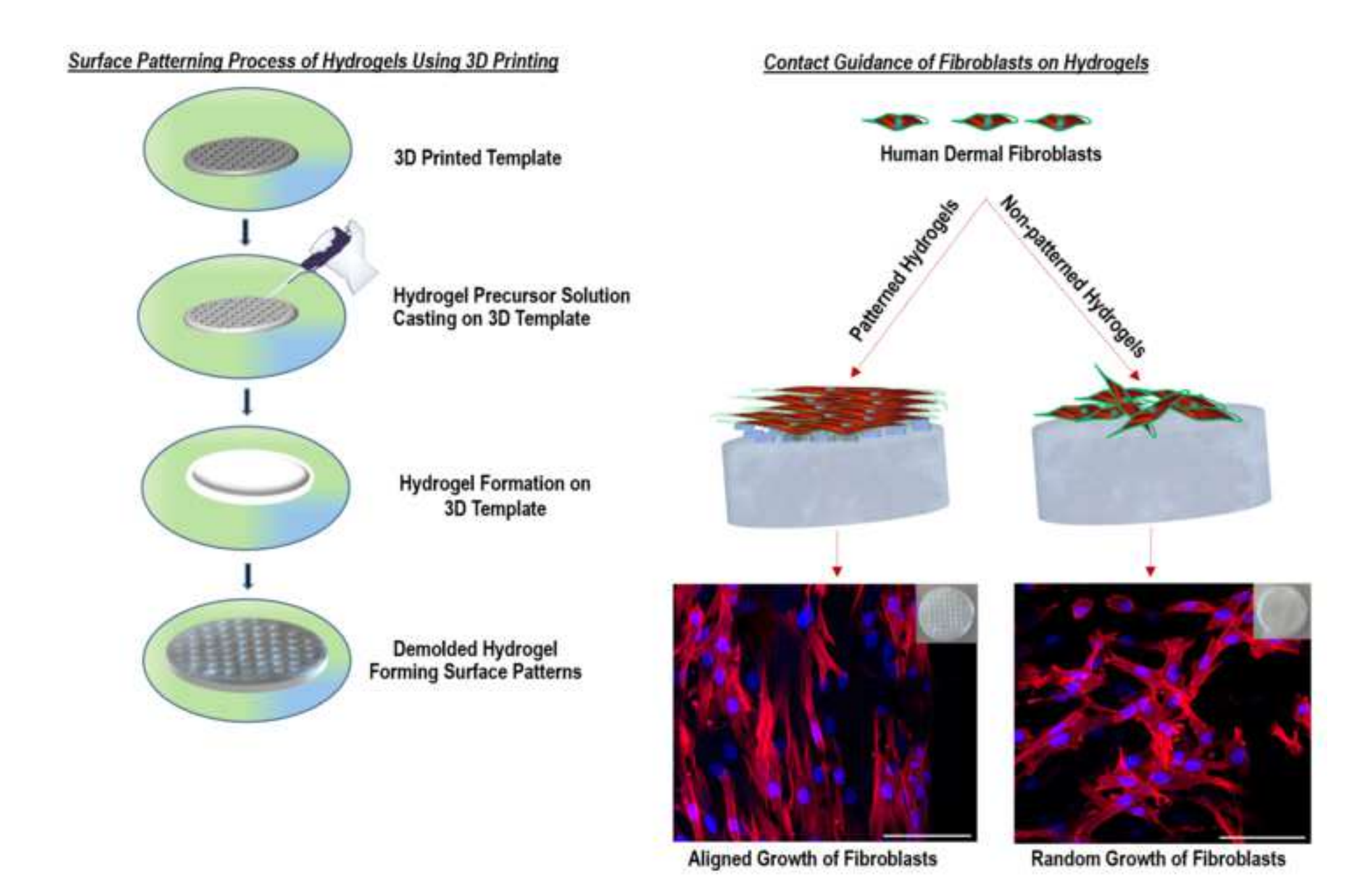
- 450 [1] E.M. Ahmed, Hydrogel: Preparation, characterization, and applications: A review, J Adv Res, 6 (2015)
- 451 105-121.
- 452 [2] T.C. Ho, C.C. Chang, H.P. Chan, T.W. Chung, C.W. Shu, K.P. Chuang, T.H. Duh, M.H. Yang, Y.C. Tyan,
- 453 Hydrogels: Properties and Applications in Biomedicine, Molecules, 27 (2022).
- 454 [3] A. Yasin, Y. Ren, J. Li, Y. Sheng, C. Cao, K. Zhang, Advances in Hyaluronic Acid for Biomedical
- 455 Applications, Front Bioeng Biotechnol, 10 (2022) 910290.
- 456 [4] Y. Piao, H. You, T. Xu, H.-P. Bei, I.Z. Piwko, Y.Y. Kwan, X. Zhao, Biomedical applications of gelatin
- 457 methacryloyl hydrogels, Engineered Regeneration, 2 (2021) 47-56.
- 458 [5] J.R. Choi, K.W. Yong, J.Y. Choi, A.C. Cowie, Recent advances in photo-crosslinkable hydrogels for
- 459 biomedical applications, BioTechniques, 66 (2019) 40-53.
- 460 [6] Y. Zhang, Y. Huang, Rational Design of Smart Hydrogels for Biomedical Applications, Frontiers in
- 461 Chemistry, 8 (2021).
- 462 [7] L. Cui, Y. Yao, E.K.F. Yim, The effects of surface topography modification on hydrogel properties, APL
- 463 Bioeng, 5 (2021) 031509.
- 464 [8] M. Ventre, P.A. Netti, Controlling Cell Functions and Fate with Surfaces and Hydrogels: The Role of
- 465 Material Features in Cell Adhesion and Signal Transduction, Gels, 2 (2016) 12.
- 466 [9] C. Leclech, C. Villard, Cellular and Subcellular Contact Guidance on Microfabricated Substrates,
- 467 Frontiers in Bioengineering and Biotechnology, 8 (2020).
- 468 [10] M.S. Hahn, L.J. Taite, J.J. Moon, M.C. Rowland, K.A. Ruffino, J.L. West, Photolithographic patterning
- of polyethylene glycol hydrogels, Biomaterials, 27 (2006) 2519-2524.
- 470 [11] M.F.A. Cutiongco, S.H. Goh, R. Aid-Launais, C. Le Visage, H.Y. Low, E.K.F. Yim, Planar and tubular
- 471 patterning of micro and nano-topographies on poly(vinyl alcohol) hydrogel for improved endothelial cell
- 472 responses, Biomaterials, 84 (2016) 184-195.
- 473 [12] S. Lv, J. Nie, Q. Gao, C. Xie, L. Zhou, J. Qiu, J. Fu, X. Zhao, Y. He, Micro/nanofabrication of brittle
- 474 hydrogels using 3D printed soft ultrafine fiber molds for damage-free demolding, Biofabrication, 12
- 475 (2020) 025015.
- 476 [13] H. Lai, B. Gong, J. Yin, J. Qian, 3D printing topographic cues for cell contact guidance: A review,
- 477 Materials & Design, 218 (2022) 110663.
- 478 [14] T.D. Clemons, M. Bradshaw, P. Toshniwal, N. Chaudhari, A.W. Stevenson, J. Lynch, M.W. Fear, F.M.
- Wood, K.S. lyer, Coherency image analysis to quantify collagen architecture: implications in scar
- 480 assessment, RSC Advances, 8 (2018) 9661-9669.

- 481 [15] F. Afghah, M. Ullah, J. Seyyed Monfared Zanjani, P. Akkus Sut, O. Sen, M. Emanet, B. Saner Okan, M.
- 482 Culha, Y. Menceloglu, M. Yildiz, B. Koc, 3D printing of silver-doped polycaprolactone-poly(propylene
- succinate) composite scaffolds for skin tissue engineering, Biomedical Materials, 15 (2020) 035015.
- 484 [16] X. Tang, Y. Qin, X. Xu, D. Guo, W. Ye, W. Wu, R. Li, Fabrication and <i>In Vitro</i> Evaluation of 3D
- Printed Porous Polyetherimide Scaffolds for Bone Tissue Engineering, BioMed Research International,
- 486 2019 (2019) 2076138.
- 487 [17] V. Fitzpatrick, Z. Martín-Moldes, A. Deck, R. Torres-Sanchez, A. Valat, D. Cairns, C. Li, D.L. Kaplan,
- 488 Functionalized 3D-printed silk-hydroxyapatite scaffolds for enhanced bone regeneration with innervation
- and vascularization, Biomaterials, 276 (2021) 120995.
- 490 [18] J. Liu, C. Su, Y. Chen, S. Tian, C. Lu, W. Huang, Q. Lv, Current Understanding of the Applications of
- 491 Photocrosslinked Hydrogels in Biomedical Engineering, Gels, 8 (2022).
- 492 [19] A. Ansari, R. Trehan, C. Watson, S. Senyo, Increasing Silicone Mold Longevity: A Review of Surface
- 493 Modification Techniques for PDMS-PDMS Double Casting, Soft Mater, 19 (2021) 388-399.
- 494 [20] O. Ursini, M. Grieco, C. Sappino, A.L. Capodilupo, S.M. Giannitelli, E. Mauri, A. Bucciarelli, C.
- 495 Coricciati, V. de Turris, G. Gigli, L. Moroni, B. Cortese, Modulation of Methacrylated Hyaluronic Acid
- 496 Hydrogels Enables Their Use as 3D Cultured Model, Gels, 9 (2023).
- 497 [21] J. Chen, Z. Wang, J. Sun, R. Zhou, L. Guo, H. Zhang, D. Liu, M. Rong, K.K. Ostrikov, Plasma-Activated
- 498 Hydrogels for Microbial Disinfection, Adv Sci (Weinh), 10 (2023) e2207407.
- 499 [22] M.E. Smithmyer, L.A. Sawicki, A.M. Kloxin, Hydrogel scaffolds as in vitro models to study fibroblast
- activation in wound healing and disease, Biomater Sci, 2 (2014) 634-650.
- 501 [23] J. Lee, A.A. Abdeen, K.L. Wycislo, T.M. Fan, K.A. Kilian, Interfacial geometry dictates cancer cell
- tumorigenicity, Nature Materials, 15 (2016) 856-862.
- 503 [24] W. Yang, Y. qin, Z. Wang, T. Yu, Y. Chen, Z. Ge, Recent advance in cell patterning techniques:
- Approaches, applications and future prospects, Sensors and Actuators A: Physical, 333 (2022) 113229.
- 505 [25] S. Shivani, Y.-H. Hsu, C.-J. Lee, C.-S. Cheong, T.-T. Chung, A.-B. Wang, Programmed Topographic
- 506 Substrates for Studying Roughness Gradient-Dependent Cell Migration Using Two-Photon
- Polymerization, Frontiers in Cell and Developmental Biology, 10 (2022).
- [26] B. Majhy, P. Priyadarshini, A.K. Sen, Effect of surface energy and roughness on cell adhesion and
- growth facile surface modification for enhanced cell culture, RSC Advances, 11 (2021) 15467-15476.
- 510 [27] A. Zareidoost, M. Yousefpour, B. Ghaseme, A. Amanzadeh, The relationship of surface roughness
- and cell response of chemical surface modification of titanium, J Mater Sci Mater Med, 23 (2012) 1479-
- 512 1488.

- [28] Q. Zhang, S. Lin, Q. Li, D. Zhao, X. Cai, Cellular Response to Surface Topography and Substrate
- 514 Stiffness, in: Y. Lin (Ed.) Cartilage Regeneration, Springer International Publishing, Cham, 2017, pp. 41-57.

Supplementary Material

Click here to access/download **Supplementary Material**Supporting Information Manuscript.docx



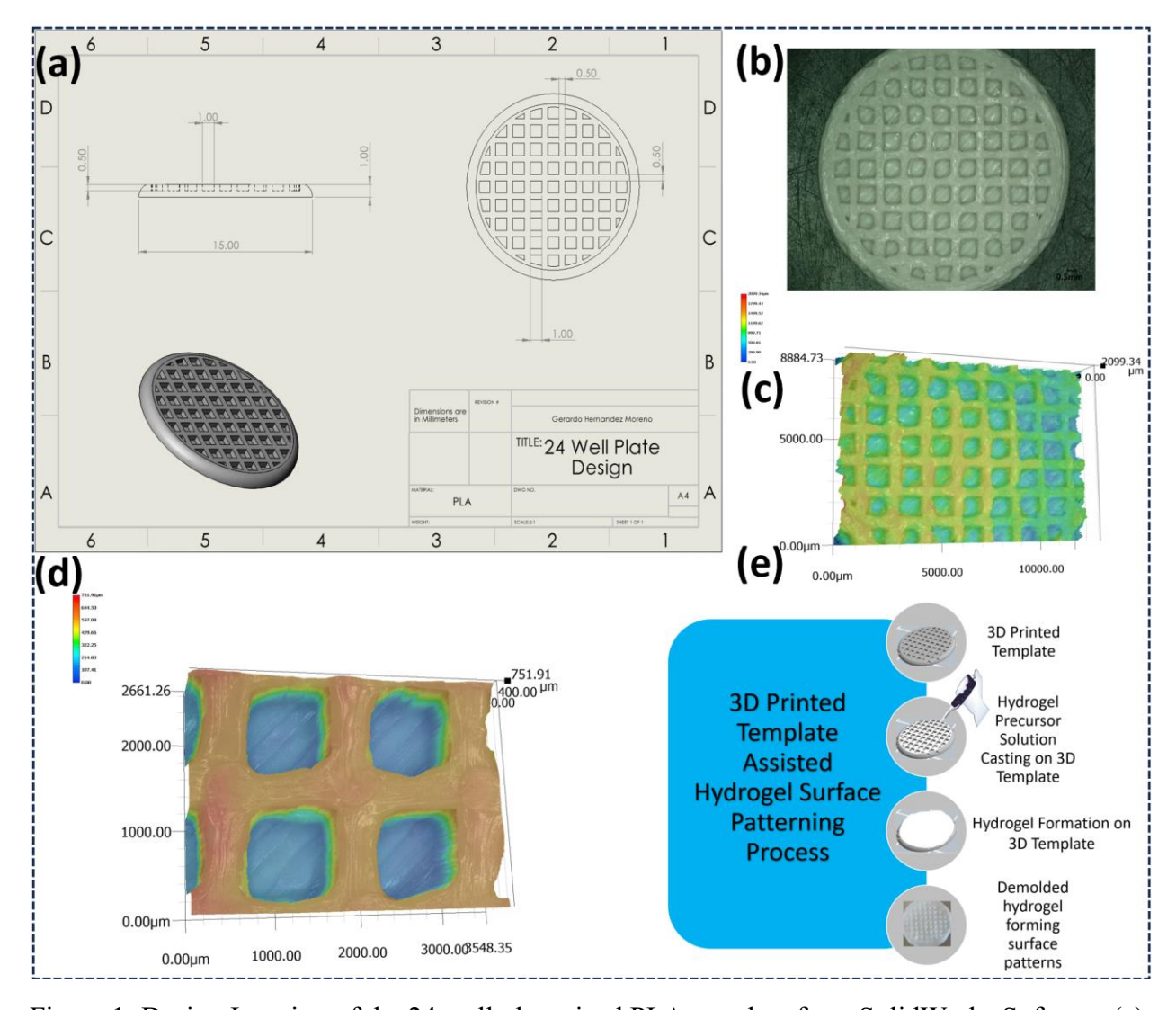


Figure 1: Design Iteration of the 24 well plate sized PLA template from SolidWorks Software (a), Laser Surface Scanning Microscopy Images of the 3D printed PLA template (b-d), 3D Laser Scanning Microscopy Images of the 3D, the schematics of the 3D printed template assisted process (e).

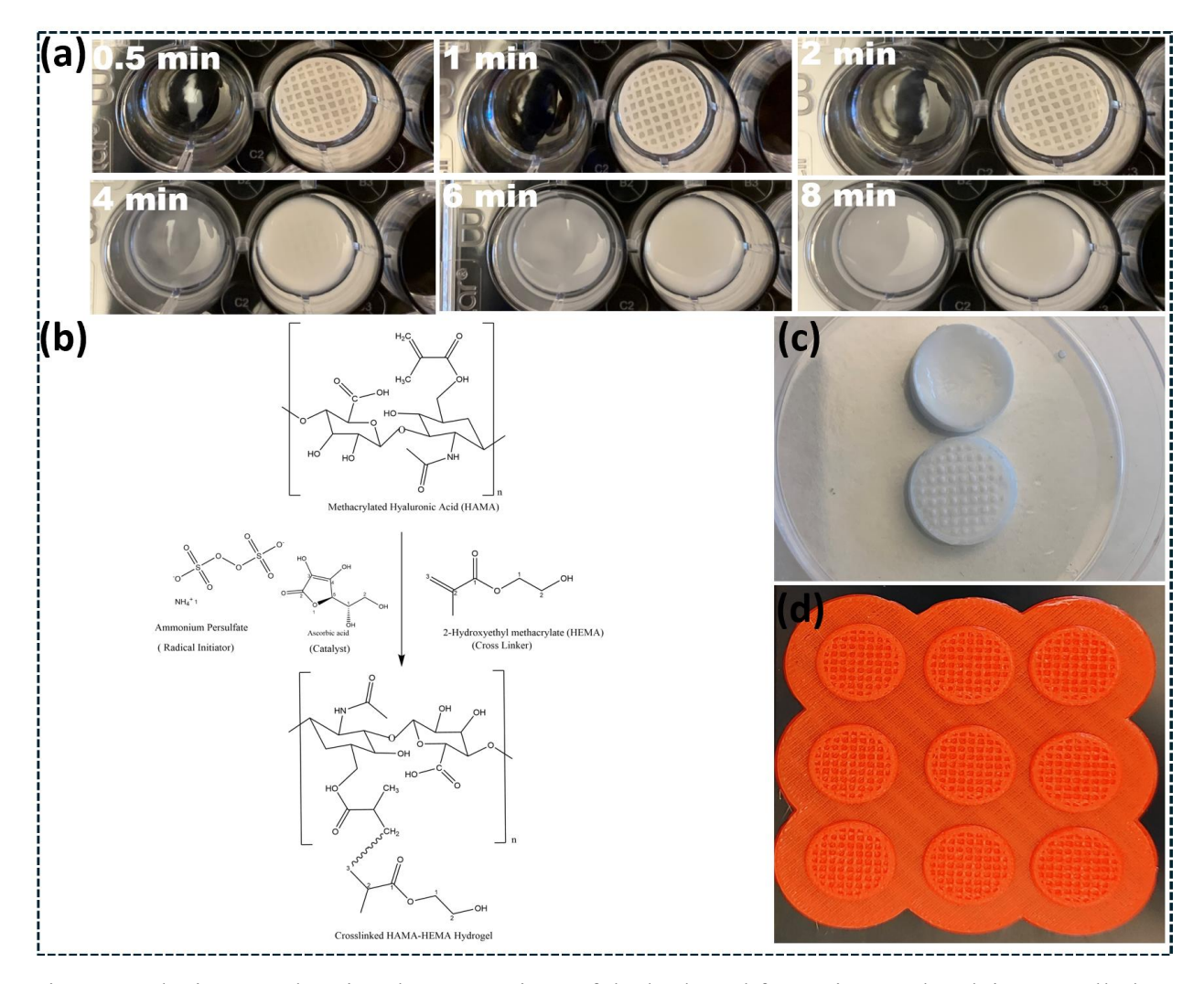


Figure 2: The images showing the comparison of the hydrogel formation on the plain 24-well plate and the top of the 3D template at different time points (a), the chemical crosslinking process of the Hyaluronic Methacrylate and 2-Hydroxy Ethyl Methacrylate forming the HA hydrogel (b), the photographs of the non-patterned and patterned hydrogels after the crosslinking process (c), image of the nine 3D printed PLA template structures (d).

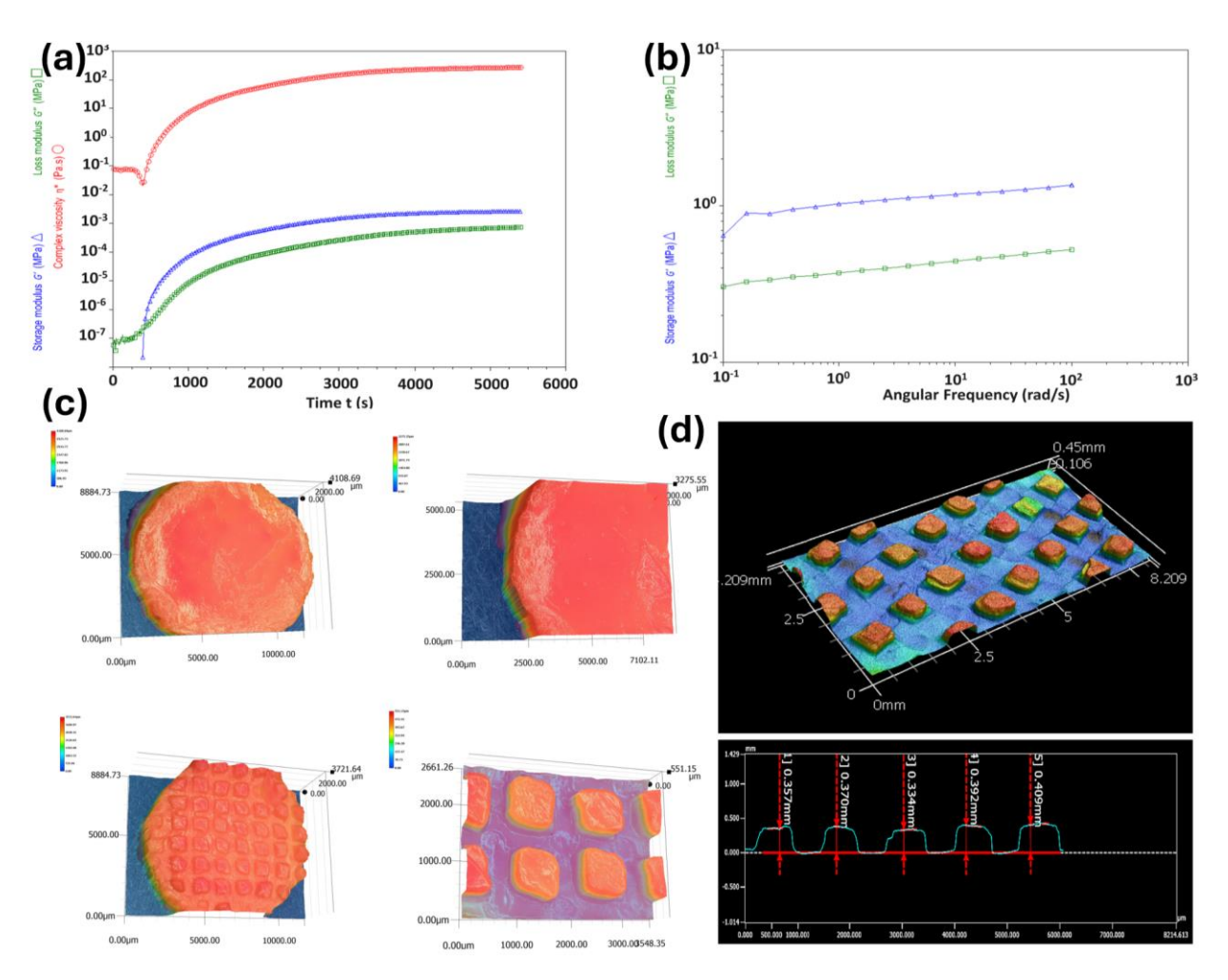


Figure 3: Rheological Measurements of HA hydrogels, time sweep experiments(a), frequency sweep experiments (b). 3D Laser Scanning Microscopy Images of the patterned and non-patterned hydrogels (to increase the contrast of the image food color dye was added on the hydrogel before taking the images) (c), Images showing the quantification of the width and height/depth of the square patterns formed on the surface of the HA hydrogels using the surface profiling measurements (d).

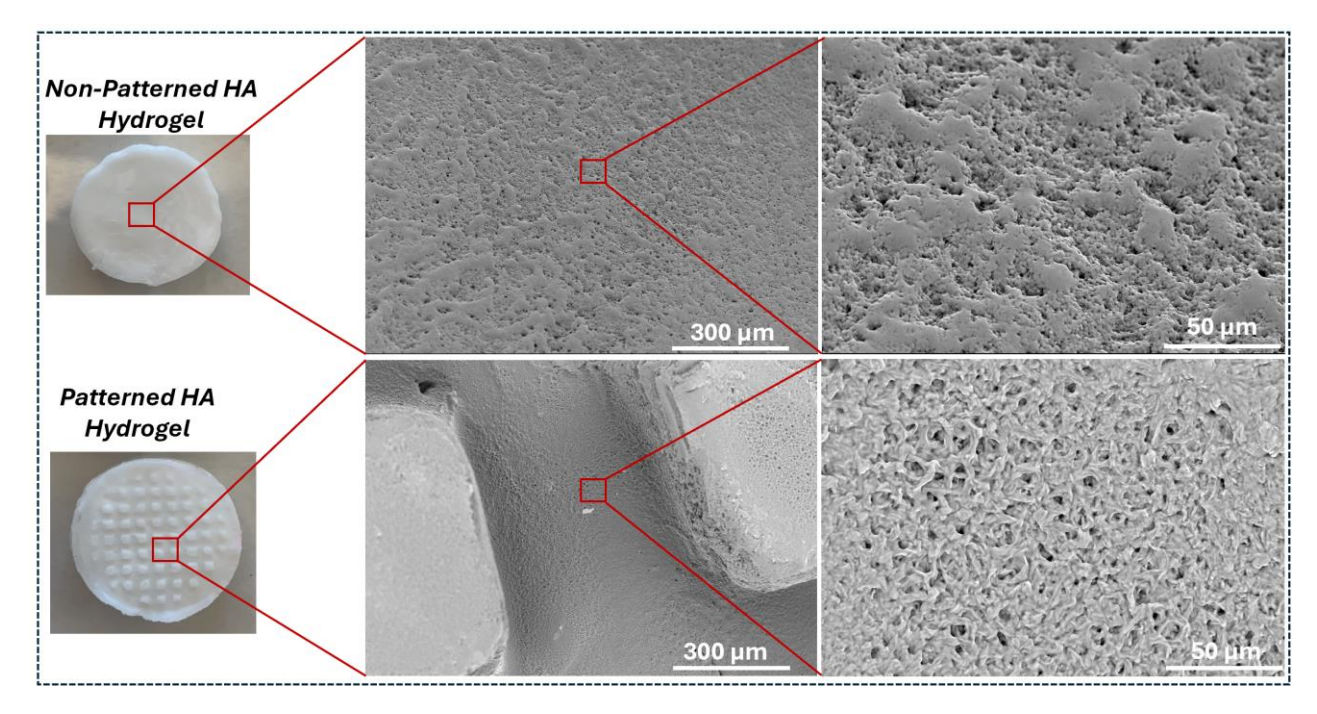


Figure 4: The Scanning Electron Microscopy Images showing the topography and pore structure of Hyaluronic Acid Methacrylate Hydrogels formed on the flat 24 well plate versus 3D printed PLA template surface

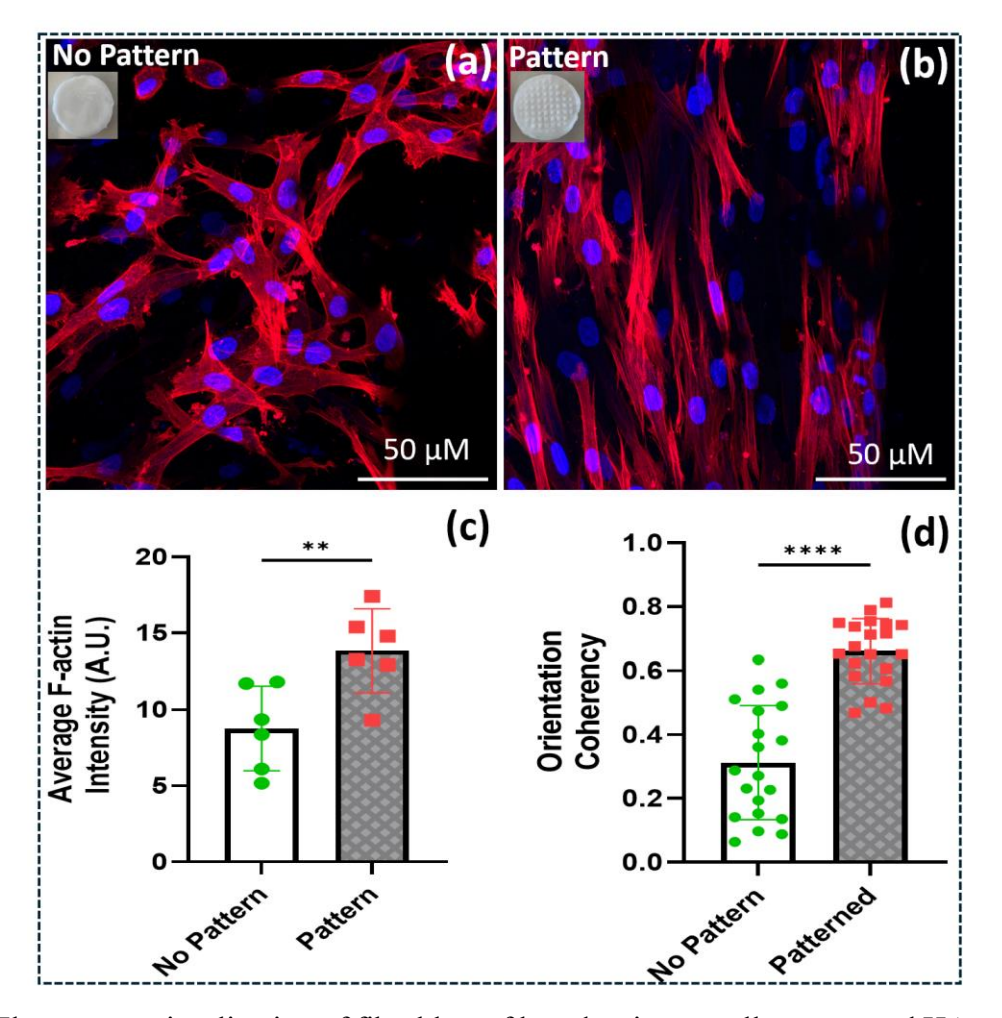


Figure 5. Fluorescent visualization of fibroblast of low density on collagen-coated HA gel without and with a surface pattern (a, b). Fluorescence images of F-actin (red) and nuclei (blue) stained human dermal fibroblast at 2 hours. (scale bars represent 50  $\mu$ m for 40x). Analysis of F-actin intensity and orientation coherency of single cells measured with ImageJ. (c, d) 0 means no alignment and 1 is perfectly aligned Measurement and comparison of the change in cell (\*P < 0.05, \*\*P < 0.01, \*\*\*P < 0.001, \*\*\*\*P < 0.0001)

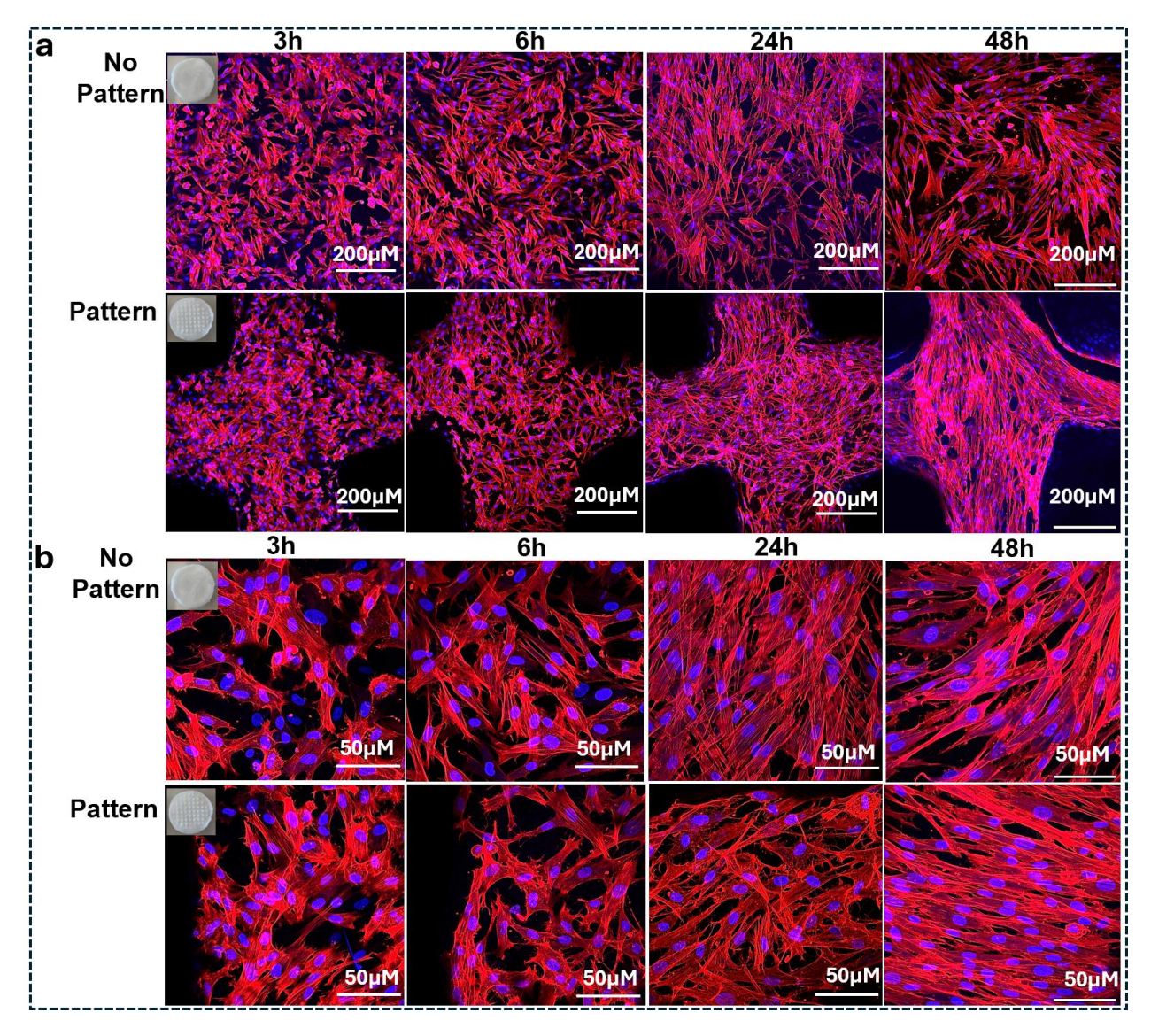


Figure 6: Fluorescent visualization of fibroblast of high density on collagen-coated HA gel with and without a surface pattern: Fluorescence images of F-actin (red) and nuclei (blue) stained human dermal fibroblast over time (1,2,3,6,24,48h) at 10 and 40X magnifications with and without a pattern (a,b). (scale bars represent  $200 \mu m$  for 10x magnification and  $50 \mu m$  for 40x).

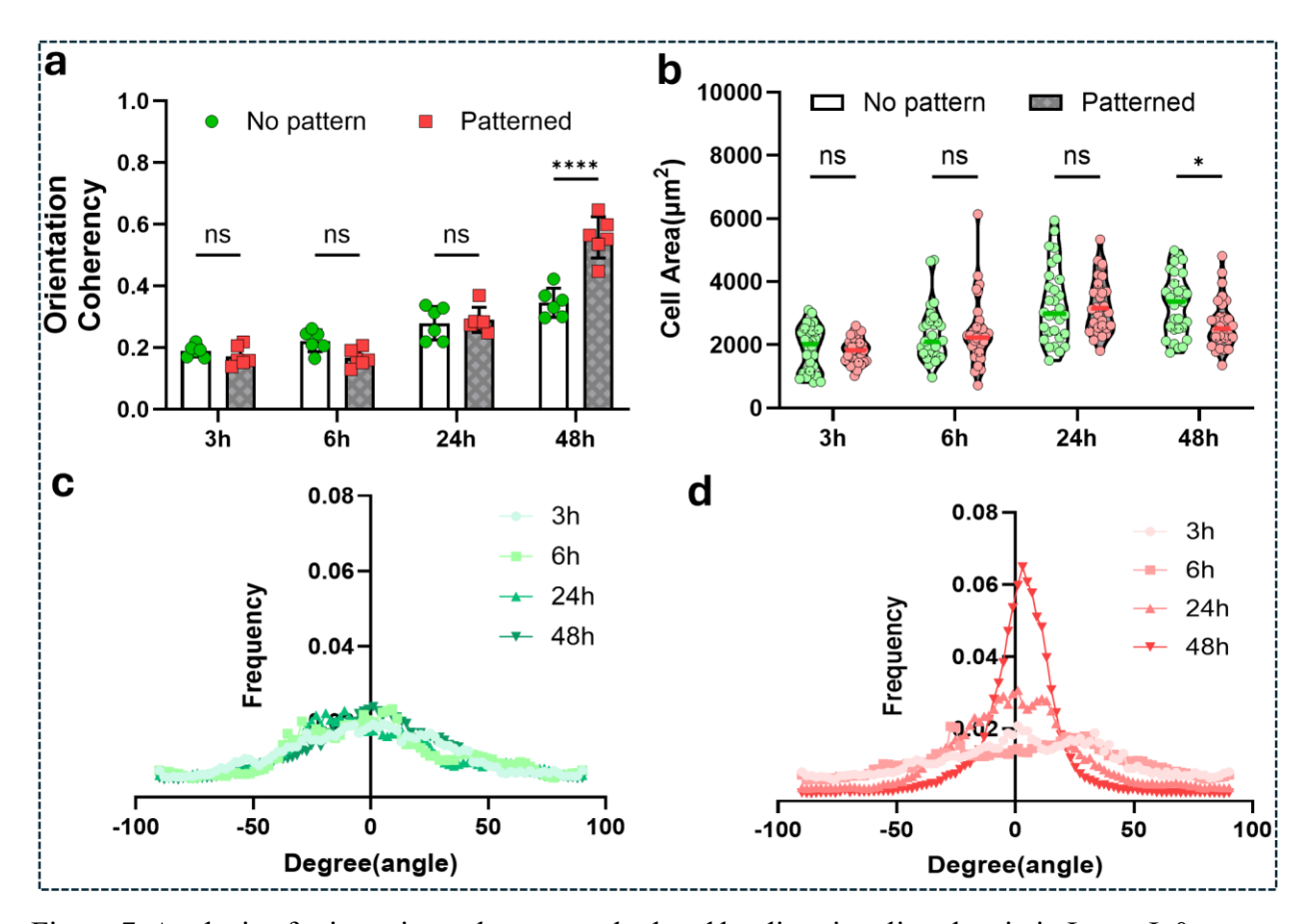


Figure 7: Analysis of orientation coherency calculated by directionality plug-in in ImageJ. 0 means no alignment and 1 is perfectly aligned (a), Measurement and comparison of the change in cell area over time for no pattern and patterned HA gel (b), Orientation distribution of stained F-actin on (c) no pattern and (d) pattered gels over time (n.s., not significant, \*P < 0.05, \*\*P < 0.01, \*\*\*\*P < 0.001, \*\*\*\*P < 0.0001).

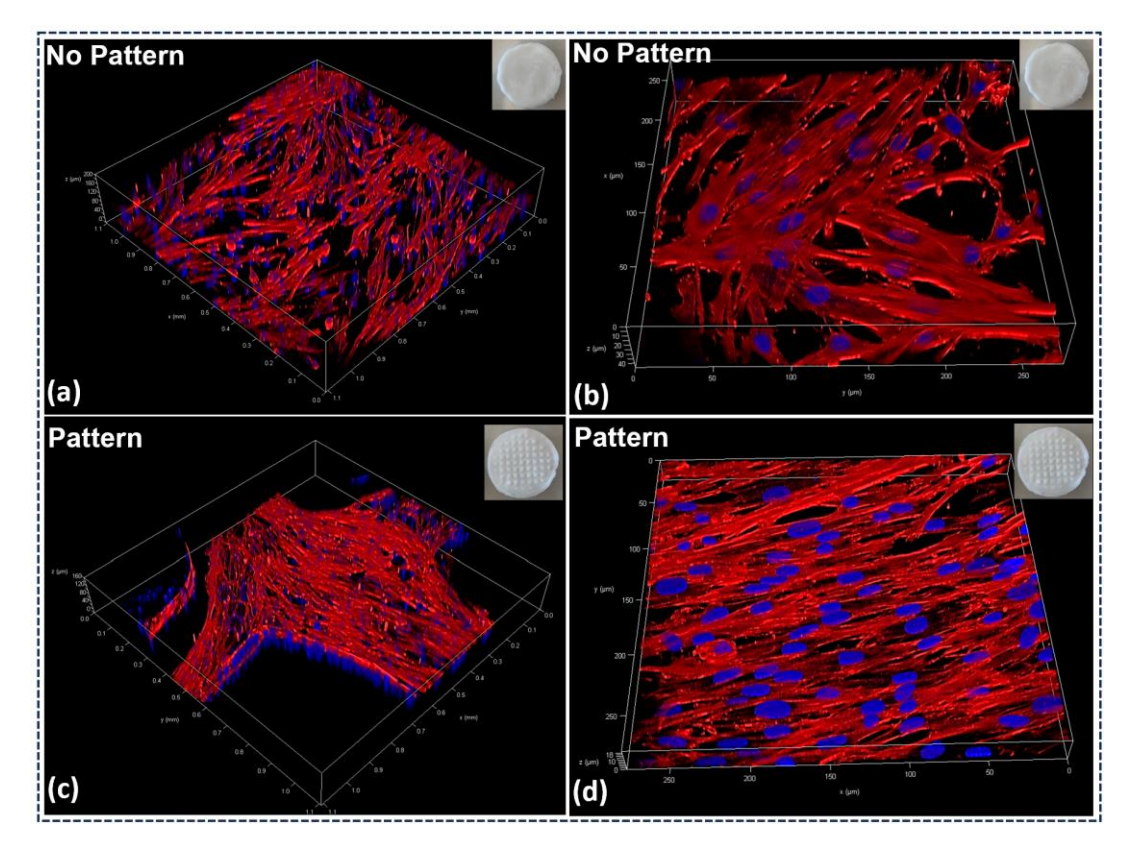


Figure 8: Z stack 3D Confocal Fluorescent images of the collagen-coated HA gel with and without a surface pattern. The images show F-actin (red) and nuclei (blue) stained human dermal fibroblast at 48h time points taken at different magnifications, 10X(a,c) and 40X (b,d).